To the Graduate Council:

I am submitting herewith a thesis written by Brenna Kay Russell entitled "Experimental Test of the Mie Theory for Microlithographically Produced Silver Spheres." I have examined the final copy of this thesis for form and content and recommend that it be accepted in partial fulfillment of the requirements for the degree of Master of Science, with a major in Physics.

Thomas L. Ferrell, Major Professor

We have read this thesis and recommend its acceptance:

Accepted for the Council:

Vice Provost
and Dean of the Graduate School

STATEMENT OF PERMISSION TO USE

In presenting this thesis in partial fulfillment of the requirements for a Master's degree at The University of Tennessee, Knoxville, I agree that the Library shall make it available to borrowers under rules of the Library. Brief quotations from this thesis are allowable without special permission, provided that accurate acknowledgment of the source is made.

Permission for extensive quotation from or reproduction of this thesis may be granted by my major professor, or in his absence, by the Head of Interlibrary Services when, in the opinion of either, the proposed use of the material is for scholarly purposes. Any copying or use of the material in this thesis for financial gain shall not be allowed without my written permission.

Signature Brenna Kay Russell

Date 11/12/86

EXPERIMENTAL TEST OF THE MIE THEORY FOR MICROLITHOGRAPHICALLY PRODUCED SILVER SPHERES

A Thesis

Presented for the

Master of Science

Degree

The University of Tennessee, Knoxville

Brenna Kay Russell

December 1986

DEDICATION

This work is dedicated to my parents, Ed and Ann, who said I could do anything I wanted to do and who lent me support throughout my life. And to my sister, Krista, who put up with the papers all over the house.

ACKNOWLEDGMENT

I wish to express my appreciation to Dr. Thomas L. Ferrell, Chairman of the thesis committee, for guidance and many helpful suggestions during the course of this investigation.

This research was supported by the Department of the Army under Interagency Agreement DOE Nos. 40-1294-82 and 3311-1450 and the Office of Health and Environmental Research, U.S. Department of Energy under contract DE-AC05-840R21400 with Martin Marietta Energy Systems, Inc.

ABSTRACT

Optical absorbance spectra were taken using microlithographically produced submicron silver spheres as samples. The spheres on each sample were of approximately uniform size, and several different samples were studied to determine the effect of sphere size on the optical absorbance. The results have been compared to theoretical calculations using Mie's scattering theory and the bulk optical properties of silver. The spheres were produced by heat treating evaporated silver on submicron quartz posts.

TABLE OF CONTENTS

CHAPTER		PAGE
I.	INTRODUCTION AND HISTORY	1
II.	THEORY	8
	A. Basic Spherical Wave Solutions of the Scalar Wave Equation	9
	B. Multipole Expansion of the Electromagnetic Fields	12
	C. Electromagnetic Scattering by a Sphere	16
III.	EXPERIMENT	22
IV.	RESULTS AND ANALYSIS	33
V.	CONCLUSION	46
REFERENCES		48
APPENDICES		51
A.	SPHERICAL BESSEL FUNCTIONS	52
B.	ANGULAR MOMENTUM OPERATOR	54
C.	SPHERICAL WAVE EXPANSION OF A VECTOR PLANE WAVE	59
VITA		62

LIST OF FIGURES

FIGURE		PAGE
1.	Silver Metal Island Film at an Angle of 50°	23
2.	Monolayer of Latex Sphere with Diameter of 482 nm	26
3.	Etch Mask of Silver Spheroids Arranged in a Semi-Ordered, Hexagonal Array	28
4.	Silicon Dioxide Posts at an Angle of 50°.	29
5.	Silver Spheres on Quartz Posts	31
6.	Absorbance Spectrum of Silver Spheres, r = 40.0 nm	35
7.	Absorbance Spectrum of Silver Spheres, r = 55.5 nm	36
8.	Absorbance Spectrum of Silver Spheres, r = 59.0 nm	37
9.	Absorbance Spectrum of Silver Spheres, r = 62.0 nm	38
10.	Absorbance Spectrum of Silver Spheres, r = 63.5 nm	39
11.	Absorbance Spectrum of Silver Spheres, r = 70 nm	40
12.	Contribution to the Absorbance Peak for Dipole Through Octupole Modes	42
13.	Retardation Curve for the Absorbance Peaks of Silver . . .	43
14.	Absorbance Peak of Spheres with 15 nm $\leq$ r $\leq$ 35 nm	46

CHAPTER I

INTRODUCTION AND HISTORY

In the field of physics submicron science focuses on the electrodynamic interactions between samples, the elastic and inelastic scattering of radiation by submicron objects, and the interaction of atoms and charged particles with submicron structures. This paper will cover an experimental test of G. Mie's [1] theory of the scattering of light from metal spheres. The investigation uses the techniques of modern submicron physics to produce samples.

Submicron physics is the physics of objects which have dimensions smaller than one micron (10^{-6} m) and larger than single atoms in size. This scale ranges from molecular physics to objects barely visible in an optical microscope.

The submicron scale was first defined by Thomas Graham [2] in 1861. He named the submicron region the "collidal scale." This term comes from the Greek word "kolla" meaning glue, which he considered a representative substance of this group. Graham was interested in the fact that when two different strengths of solutions are separated by a permeable membrane they will in time become uniformly blended such that the strength of the solution on both sides of the membrane is the same. He experimented with several different substances and discovered that although a solution of salt or sugar will diffuse, a solution of glue or gelatin will not. He concluded that there are certain

substances with particles too large to diffuse through the membrane, and there are certain substances with particles small enough to penetrate the membrane. Substances which in solution will pass through a membrane are called crystalline solids. They exist in a solvent as molecules, atoms, or ions and form a "true" solution. Substances composed of particles which in solution are too large to pass through a standard membrane he named colloids; hence, the name colloidal scale.

The first known usage of colloid particles was in the Middle Ages. Alchemists used a substance known to them as "aurum potabile," or "drinkable gold." While searching for ways to make gold out of less valuable metal they stumbled across a method of reducing the size of gold particles to what is known today as a few nanometers in size. The particles were too small to settle out, thus a colloidal aqueous solution, or "sol," was formed. A French chemist, Macquer, was the first to state that the drinkable gold solution is not a true solution because unlike salt and sugar, the gold solution contains particles larger than molecules. One of the samples to which the Mie theory was first applied was gold sols.

Faraday hypothesized that although he could not see the individual particles of a colloidal gold solution in an optical microscope, the solution is not a true solution. He knew that, when a ray of sunlight passes through a semi-darkened room, the air is visible by the reflected light. He used this same idea in his work on solutions. When he passed a beam of focused light through a solution of colloidal gold the light cut a visible path. However, when pure

water and a true solution were used no such path was observed. His experiments proved two facts: (1) solid matter does exist in a very finely subdivided condition with the particle size ranging between the microscopic and the molecular and (2) the presence of these particles can be detected by passing a beam of light through a sol and seeing the scattered or reflected light. Faraday was joined by John Tyndall, who did further work on the project. The white path that is formed when a beam is shone through a colloidal solution is known today as a Tyndall cone [3].

The electromagnetic scattering work of Faraday and Tyndall was made quantitative by Lord Rayleigh [4] in the late 1800s, and by the early 1900s Mie's theory of light scattering by spheres had been published. Mie's theory included absorbance, as well as the "blue sky" scattering analysis of Rayleigh, so that the color of sol particulates which repel surrounding particulates could be correlated with particulate sizes smaller than the wavelength of light. These works attracted some work by several others such as Einstein, Debye, Perrin, and Von Smoluchowske. Einstein's work included his famous treatment of Brownian motion [5] (he found that the effects are greater for smaller particulates). This was quantitatively verified by Perrin in 1913. Einstein also contributed to the theory of diffusion, which allowed calculation of sol sedimentation rates and rates of gaseous diffusion through micropores. Debye and Huckel [6], in 1923, worked out the equations for the electrical potential surrounding an ion in

solutions. The theory permits an understanding of the energy of repulsion which keeps sol particulates apart.

Also in 1923, T. Svedberg [7] developed the ultracentrifuge. Colloidal particles are so small that Brownian motion prevents them from settling due to gravity. Svedberg decided to use an effect that resembles gravitation—the centrifugal effect. He developed the ultracentrifuge to separate colloidal particles (the ultracentrifuge spins so fast that an effect equivalent to hundreds of thousands of times normal gravity results). From the rate of settling the size could be deduced. By varying the speed of rotation a mixture of two different types of particles could be separated.

Zsigmondy, like Svedberg, developed a new tool to study colloids. Zsigmondy, an organic chemist, realized that since colloidal particles are large enough to show the Tyndall effect, maybe the scattered light could be used to see the particles. If light was shone through a colloidal solution and if a microscope was adjusted at right angles to the beam, then only scattered light would enter the microscope; therefore, even if the particles could not be seen clearly, they could at least be seen as points of light and could be studied. From this the size and the shape could be deduced. This instrument was called the ultramicroscope [8]. In 1932 Ruska invented the electron microscope [9]. As a result, scientists were able to see the size and shape of submicron particles in detail.

Today colloidal science spans across chemistry and physics. Chemists refer to it as the domain of high polymers. In addition to

polymers, they are also interested in surface catalysis, emulsions and sols. Surface catalysis by submicron particles and structures is widely used in industry. This is because there is a much larger surface area presented by a collection of small particles than by the same mass of bulk material. Some examples of the uses of colloidal catalysis in chemistry are the cracking of petroleum, the production of sulfuric acid, and hydrogenation. The chemists divide colloids into two groups: sols and gels. Sols are colloidal particulates which repel surrounding water. Gels such as glues, starches, pectin, gelatin, and egg whites are particulates which attract water.

Physicists study the physical implications of colloids, such as how they interact and the elastic and inelastic scattering of radiation by colloidal particles. This allows investigation into differences between bulk material and colloidal particles. Work being done now on colloidal particulates includes the cause of the colors of colloidal metals, electrostatic interaction between spherical colloidal particles, refraction by spherical colloidal particles, and light scattering from colloidal dispersions.

In 1908 Mie published his paper on electromagnetic scattering theory using Maxwell's equations and the associated boundary conditions for spheres. His theory predicts not only an absorbance peak for the dipole mode, $\ell=1$ mode of a multipole expansion, but also absorbance peaks due to higher order modes ($\ell=2,3,\ldots$). This work has led to the publication of many papers about the theory and possible extension and corrections of the theory. S. Martinos [10] recently hypothesized

that there would be effects in the absorbance spectra due to the excitation of special surface plasma modes. If he is correct, then when the absorption spectrum of silver spheres is taken, there should be additional peaks not predicted by Mie. As will be shown later, this effect was not seen in the experimental data.

R. Ruppin [11] has proposed an extension to Mie's theory when dealing with spheres that have a radius of less than 20 nm. This extension allows for the excitation of longitudinal polarization waves. This leads, in theory, to a slight shift in the main plasma resonance from its normal position (calculated from Mie's theory) to a higher frequency. For a radius greater than 20 nm the extension deviates very little from the results of Mie's theory. The present work is unable to resolve these deviations.

Boardman and Paranjape [12] have studied optical surface modes of metal spheres in their calculations. Papers dealing with calculations of Mie's theory—such as Grehan and Gouesbet [13], Evans [14], Drake and Gordon [15], Bar-Isaac and Hardy [16], Vafin and Dregalin [17], and Gordon [18]—all deal with the corrections and extensions of this theory. Papers by Ganiere et al. [19] and Smithard [20] on theoretical checks on Mie's theory using the quantum mechanical theory of Kawakata and Kubo [21] discuss sizing of spheres. Surface enhanced Raman scattering of colloidal particles as it relates to Mie's theory has been discussed by Kerker et al. [22], Kerker and Druger [23], Wang et al. [24], and Chang et al. [25]. However, a systematic experimental proof on Mie's theory has not been done. In the next

chapter Mie's scattering theory is discussed for reference purposes. The scattering of waves from a sphere with a local dielectric function is presented, which leads to the cross section for scattering by the spheres. Following this the experimental results are compared to the theoretical results.

CHAPTER II

THEORY

Metals not only exhibit optical characteristics in bulk, they also display them in particulate form, such as colloidal suspensions. In the colloidal state, reflection, absorption, and diffraction all take place side by side.

Since metals are neither perfectly conducting nor perfectly transparent at optical frequencies, one cannot treat scattering by metal particles using simple diffraction. Absorption must be taken into consideration.

When an electromagnetic wave is incident on a sphere that is much smaller than the wavelength, the sphere sees the speed of light to be effectively infinite because the oscillation across the sphere is practically instantaneous from one side of the sphere to the other. As the size is increased it takes an increasingly larger amount of time for the oscillation to cross the sphere, and the sphere sees the speed of light as finite. This retardation has an effect on absorption. When this occurs the theoretical explanation must rigorously include Maxwell's equations. As the retardation increases a correction to the nonretarded solution must include the term $(\omega a/c)^2$ and higher powers, where ω is the angular frequency of the light, a is the sphere radius, and c is the speed of light. Mie was interested in investigating the color of metal colloids and in Rayleigh

scattering. In his investigation of these matters he calculated the general cross section for scattering of light incident on metallic spheres.

The Mie solution, although derived for scattering by a single sphere, can also apply to diffraction by a collection of spheres which are randomly distributed and sufficiently well separated. If this is the case there are no coherent phase relationships between the light that is scattered by the different spheres, and the total scattered energy is then equal to the energy scattered by one sphere multiplied by their total number.

In deriving Mie's theory [26] solutions to the scalar wave equation, multipole expansion of the electromagnetic fields, the spherical wave expansion of a vector plane wave, and scattering of electromagnetic waves by a sphere are found.

A. BASIC SPHERICAL WAVE SOLUTIONS OF THE SCALAR WAVE EQUATION

In dealing with the vector spherical wave problem we must first consider the scalar wave equation:

$$\nabla^2\psi - \frac{1}{c^2}\frac{\partial^2\psi}{\partial t^2} = 0 \tag{1}$$

where $\psi(\underset{\sim}{r},t)$ satisfies the source-free wave equation and the Fourier transform in time is:

$$\psi(\underset{\sim}{r},t) = \int_{-\infty}^{\infty}\psi(\underset{\sim}{r},\omega)e^{-i\omega t}d\omega \tag{2}$$

and each Fourier component satisfies the Helmholtz equation

$$(\nabla^2 + K^2)\psi(\underset{\sim}{r},\omega) = 0 \tag{3}$$

where $K^2 = \omega^2/c^2$.

Since we are interested in the spherical problem we put the equations in spherical coordinates (r,θ,ϕ). The Laplace equation can be written in spherical coordinates as:

$$\frac{1}{r}\frac{\partial^2}{\partial r^2}(r\psi) + \frac{1}{r^2\sin\theta}\frac{\partial}{\partial\theta}(\sin\theta\frac{\partial\psi}{\partial\theta}) + \frac{1}{r^2\sin^2\theta}\frac{\partial^2\psi}{\partial\phi^2} = 0 \ . \tag{4}$$

The separation of the angular and radial variables for the Helmholtz equation is gained by writing

$$\psi(\underset{\sim}{r},\omega) = \sum_{\ell m} f_\ell(Kr)Y_{\ell m}(\theta,\phi) \tag{5}$$

where the spherical harmonics are introduced as

$$Y_{\ell m}(\theta,\phi) = \sqrt{\frac{2\ell+1}{4\pi}\frac{(\ell-m)!}{(\ell+m)!}}\,P_\ell^m(\cos\theta)e^{im\phi} \tag{6}$$

and the associated Legendre function is

$$P_\ell^m(x) = (-1)^m(1-x^2)^{m/2}\frac{d^m}{dx^m}P_\ell(x) \tag{7}$$

where $x = \cos\theta$ and $P_\ell(x)$ is the Legendre polynomial of order 1. The radial functions $f_\ell(Kr)$ satisfy the radial equation, independent of m,

$$\left[\frac{d^2}{dr^2} + \frac{2}{r}\frac{d}{dr} + K^2 - \frac{\ell(\ell+1)}{r^2}\right] f_\ell(Kr) = 0 \ . \tag{8}$$

With the substitution

$$f_\ell(Kr) = \frac{1}{r^{1/2}}\, u_\ell(Kr) \tag{9}$$

Equation (8) is

$$\left[\frac{d^2}{dr^2} + \frac{1}{r}\frac{d}{dr} + K^2 - \frac{(\ell+\frac{1}{2})^2}{r^2}\right] u_\ell(Kr) = 0 \tag{10}$$

This equation is simply the Bessel equation

$$\left[\frac{d^2}{dr^2} + \frac{1}{r}\frac{d}{dr} + (K^2 - \frac{\nu^2}{r^2})\right] u_\ell(Kr) = 0 \tag{11}$$

where $\nu = \ell + \frac{1}{2}$. Therefore the solution for $f_\ell(Kr)$ is

$$f_\ell(Kr) = \frac{A_{\ell m}}{r^{1/2}}\, J_{\ell+1/2}(Kr) + \frac{B_{\ell m}}{r^{1/2}}\, N_{\ell+1/2}(Kr) \ . \tag{12}$$

The spherical Bessel and Hankel functions, denoted by $j_\ell(Kr)$, $n_\ell(Kr)$ and $h_\ell^{(1,2)}(Kr)$ are convenient to introduce here. They are

$$\left.\begin{aligned} j_\ell(Kr) &= (\tfrac{\pi}{2Kr})^{1/2}\, J_{\ell+1/2}(Kr) \\ n_\ell(Kr) &= (\tfrac{\pi}{2Kr})^{1/2}\, N_{\ell+1/2}(Kr) \\ h_\ell^{(1,2)}(Kr) &= (\tfrac{\pi}{2Kr})^{1/2}[J_{\ell+1/2}(Kr) \pm i N_{+1/2}(Kr)] \end{aligned}\right\} \ . \tag{13}$$

The general solution of Eq. (3) in spherical coordinates can be written as

$$\psi(\underset{\sim}{r}) = \sum_{\ell m} [A_{\ell m}^{(1)} \, h_{\ell}^{(1)}(Kr) + A_{\ell m}^{(2)} \, h_{\ell}^{(2)}(Kr)] Y_{\ell m}(\theta,\phi) \tag{14}$$

where the coefficients $A_{\ell m}^{(1)}$ and $A_{\ell m}^{(2)}$ will be determined by boundary conditions.

Attention is now turned to the angular functions. The basic angular functions are the spherical harmonics [6] which are the solutions of the eigenequation

$$- \left[\frac{1}{\sin\theta} \frac{\partial}{\partial\theta} \left(\sin\theta \frac{\partial}{\partial\theta}\right) + \frac{1}{\sin^2\theta} \left(\frac{\partial^2}{\partial\phi^2}\right)\right] Y_{\ell m}(\theta,\phi) = \ell(\ell+1) Y_{\ell m}(\theta,\phi) \, . \tag{15}$$

This equation can be written in the form

$$\hat{\underset{\sim}{L}}^2 \, Y_{\ell m}(\theta,\phi) = \ell(\ell+1) Y_{\ell m}(\theta,\phi) \, . \tag{16}$$

The differential operator $\hat{L}^2 = L_x^{\,2} + L_y^{\,2} + L_z^{\,2}$, where

$$\hat{\underset{\sim}{L}} = \frac{1}{i} \left(\underset{\sim}{r} \times \underset{\sim}{\nabla}\right) \tag{17}$$

is $\hbar^{-1}$ times the orbital angular-momentum operator of wave mechanics.

B. MULTIPOLE EXPANSION OF THE ELECTROMAGNETIC FIELDS

If one assumes the time dependence $e^{-i\omega t}$, and the time independent parts of both the electric and magnetic vectors inside and

outside the sphere satisfy Maxwell's equations in their time-free form, then

$$\nabla \times \underset{\sim}{E} = i\,Kc\,\underset{\sim}{B} \tag{18a}$$

$$\nabla \times \underset{\sim}{B} = -i\,\frac{K}{c}\,\underset{\sim}{E} \tag{18b}$$

$$\nabla \cdot \underset{\sim}{E} = 0 \tag{18c}$$

$$\nabla \cdot \underset{\sim}{B} = 0 \tag{18d}$$

in SI units $K = \omega/c$. Eliminating $\underset{\sim}{E}$ by combining Eq. (18a) and (18b) we obtain

$$(\nabla^2 + K^2)\underset{\sim}{B} = 0 \ . \tag{19}$$

Similarly, by eliminating $\underset{\sim}{B}$ we obtain

$$(\nabla^2 + K^2)\underset{\sim}{E} = 0 \ . \tag{20}$$

We want to find the multipole solution for $\underset{\sim}{E}$ and $\underset{\sim}{B}$. We will follow the procedure suggested by Bouwokamp and Casimir. One can easily verify for a given vector field $\underset{\sim}{A}$

$$\nabla^2(\underset{\sim}{r} \cdot \underset{\sim}{A}) = \underset{\sim}{r} \cdot (\nabla^2\underset{\sim}{A}) + 2\nabla \cdot \underset{\sim}{A} \ . \tag{21}$$

From Eq. (18) it follows that the scalars $\underset{\sim}{r} \cdot \underset{\sim}{E}$ and $\underset{\sim}{r} \cdot \underset{\sim}{B}$ satisfy the Helmholtz wave equations

$$(\nabla^2 + K^2)(\underset{\sim}{r} \cdot \underset{\sim}{E}) = 0 \ , \tag{22a}$$

$$(\nabla^2 + K^2)(\underset{\sim}{r} \cdot \underset{\sim}{B}) = 0 \ . \tag{22b}$$

The general solution for Eq. (22a) and Eq. (22b) is given by Eq. (14). We now define a magnetic multipole field of order (ℓ,m) by the conditions

$$\underset{\sim}{r} \cdot \underset{\sim}{B}^{(M)}_{\ell n} = \frac{\ell(\ell+1)}{K}\, g_\ell(Kr) Y_{\ell m}(\theta,\phi) \tag{23a}$$

$$\underset{\sim}{r} \cdot \underset{\sim}{E}^{(M)}_{\ell m} = 0 \tag{23b}$$

where

$$g_\ell(Kr) = A^{(1)}_\ell\, h^{(1)}_\ell(Kr) + A^{(2)}_\ell\, h^{(2)}_\ell(Kr) \ . \tag{24}$$

Using Eq. (18a) we can relate $\underset{\sim}{r} \cdot \underset{\sim}{B}$ to $\underset{\sim}{E}$:

$$\begin{aligned} K\underset{\sim}{r} \cdot \underset{\sim}{B} &= \frac{1}{i}\, \underset{\sim}{r} \cdot (\underset{\sim}{\nabla} \times \underset{\sim}{E}) \\ &= \frac{1}{i}\, (\underset{\sim}{r} \times \underset{\sim}{\nabla}) \cdot \underset{\sim}{E} \\ &= \underset{\sim}{L} \cdot \underset{\sim}{E} \end{aligned} \tag{25}$$

where $\underset{\sim}{L}$ is given by (17). By equating Eq. (23a) and Eq. (25) we have

$$\underset{\sim}{L} \cdot \underset{\sim}{E}^{(M)}_{\ell m} = \ell(\ell+1) g_\ell(Kr) Y_{\ell m}(\theta,\phi) \ . \tag{26}$$

To determine the purely transverse electric field we use Eq. (26), knowing that the operator $\underset{\sim}{L}$ acts only on the angular variables. The radial dependence of $\underset{\sim}{E}^{(M)}_{\ell m}$ is given by $g_\ell(Kr)$. Also, the operator $\underset{\sim}{L}$ acting on $Y_{\ell m}$ transforms the azimuthal value according to Eq. (B.5) and does not change the multipole index. So the components

of $\underset{\sim}{E}^{(M)}_{\ell m}$ can be at most linear combinations of $Y_{\ell m}$ with different m values and a common multipole index which is equal to the value of the multipole index on the right-hand side of Eq. (26). In order for $\underset{\sim}{L} \cdot \underset{\sim}{E}^{(M)}_{\ell m}$ to yield a single $Y_{\ell m}$ the components of $\underset{\sim}{E}^{(M)}_{\ell m}$ must compensate for whatever raising or lowering of m values are caused by the operator $\underset{\sim}{L}$. Thus the electric field should be

$$\underset{\sim}{E}^{(M)}_{\ell m} = g_\ell(Kr)\underset{\sim}{L}\, Y_{\ell m}(\theta,\phi) \ . \tag{27}$$

Together Eq. (27) and Eq. (18a) specify the electromagnetic fields of a magnetic multipole of order (ℓ,m).

In the electric multipole fields:

$$\underset{\sim}{B}^{(E)}_{\ell m} = f_\ell(Kr)\underset{\sim}{L}\, Y_{\ell m}(\theta,\phi) \tag{28a}$$

$$\underset{\sim}{E}^{(E)}_{\ell m} = \frac{i}{K}\, \underset{\sim}{\nabla} \times \underset{\sim}{B}^{(E)}_{\ell m} \tag{28b}$$

where $f_\ell(Kr)$ is similar to $g_\ell(Kr)$. When we combine the two types of fields we can write the general solution to Maxwell's equation [3]:

$$\begin{aligned} \underset{\sim}{B} &= \sum_{\ell m} \left[a_E(\ell m) f_\ell(Kr)\underset{\sim}{\chi}_{\ell m} - \frac{i}{K}\, a_M(\ell m)\underset{\sim}{\nabla} \times g_\ell(Kr)\underset{\sim}{\chi}_{\ell m}\right] \\ \underset{\sim}{E} &= \sum_{\ell m} \left[\frac{i}{K}\, a_E(\ell m)\underset{\sim}{\nabla} \times f\,(Kr)\underset{\sim}{\chi}_{\ell m} + a_M(\ell m) g_\ell(Kr)\underset{\sim}{\chi}_{\ell m}\right] . \end{aligned} \tag{29}$$

a_E and a_M can be found by

$$\begin{aligned} a_M(\ell m) g_\ell(Kr) &= \frac{K}{\sqrt{\ell(\ell+1)}} \int Y^*_{\ell m}(\theta,\phi)\underset{\sim}{r} \cdot \underset{\sim}{B}\, d\Omega \\ a_E(\ell m) f_\ell(Kr) &= \frac{K}{\sqrt{\ell(\ell+1)}} \int Y^*_{\ell m}(\theta,\phi)\underset{\sim}{r} \cdot \underset{\sim}{E}\, d\Omega \end{aligned} \tag{29a}$$

so if one knows $\underset{\sim}{r} \cdot \underset{\sim}{B}$ and $\underset{\sim}{r} \cdot \underset{\sim}{E}$ at two different radii, r_1 and r_2, in a source free region it will allow a complete specification of the fields including determination of the relative proportions of $h_\ell^{(1)}$ and $h_\ell^{(2)}$ in f_ℓ and g_ℓ.

C. ELECTROMAGNETIC SCATTERING BY A SPHERE

Consider a sphere with radius a and propagation constant K_1 to be embedded in an infinite, homogeneous medium with propagation constant K_2. A plane wave whose electric field is linearly polarized in the x-direction is propagated along the z-axis. The incident electric and magnetic fields [27] with their amplitudes and time dependence factored out can be written as

$$\underset{\sim}{E}_i(\underset{\sim}{r}) = \sum_{\ell=1}^{\infty} \sum_{m=\pm 1} i^\ell \sqrt{\pi(2\ell+1)} \left(\underset{\sim}{U}_{\ell m}^{(1)}(K_2\vec{r}) + m \frac{1}{K_2} \underset{\sim}{\nabla} \times \underset{\sim}{U}_{\ell m}^{(1)}(K_2\vec{r}) \right) \tag{30}$$

$$\underset{\sim}{B}_i(\underset{\sim}{r}) = \frac{K_2}{\omega} \sum_{\ell=1}^{\infty} \sum_{m=\pm 1} m\, i^{\ell+1} \sqrt{\pi(2\ell+1)} \left(\underset{\sim}{U}_{\ell m}^{(1)}(K_2,\vec{r}) + m \frac{1}{K_2} \underset{\sim}{\nabla} \times \underset{\sim}{U}_{\ell m}^{(1)}(K_2,\vec{r}) \right)$$

where

$$\underset{\sim}{U}_{\ell m}^{(j)}(K,\vec{r}) = - F_\ell^{(j)}(Kr) \chi_{\ell m}(\theta,\phi) \ , \tag{31}$$

$$\begin{aligned} F_\ell^{(j)}(Kr) &= j_\ell(Kr) \quad , \quad j = 1 \\ F_\ell^{(j)}(Kr) &= h_\ell^{(1)}(Kr) \quad , \quad j = 3 \end{aligned} \tag{32}$$

and $\chi_{\ell m}(\theta,\phi)$ is given in (B.13). The induced fields are constructed in two parts, one applying to the inside of the sphere and the

other to the outside of the sphere:

$$\underset{\sim}{E}_{out}(\underset{\sim}{r}) = \sum_{\ell=1}^{\infty} \sum_{m=\pm 1} i^{\ell}\sqrt{\pi(2\ell+1)}\left[a_{\ell}\,\underset{\sim}{U}^{(3)}_{\ell m}(K_2,\vec{r}) + b_{\ell}\,m\,\frac{1}{K_2}\underset{\sim}{\nabla}\times\underset{\sim}{U}^{(3)}_{\ell}(K_2,\vec{r})\right] \tag{33}$$

$$\underset{\sim}{B}_{out}(\underset{\sim}{r}) = -\frac{K_2}{\omega}\sum_{\ell=1}^{\infty}\sum_{m=\pm 1} mi^{\ell+1}\sqrt{\pi(2\ell+1)}\;\left[b_{\ell}\,\underset{\sim}{U}^{(3)}_{\ell m}(K_2,\vec{r}) + a_{\ell}\,m\,\frac{1}{K_2}\underset{\sim}{\nabla}\times\underset{\sim}{U}^{(3)}_{\ell m}(K_2,\vec{r})\right]$$

for $r > a$.

$$\underset{\sim}{E}_{in}(\underset{\sim}{r}) = \sum_{\ell=1}^{\infty} \sum_{m=\pm 1} i^{\ell}\sqrt{\pi(2\ell+1)}\left[c_{\ell}\,\underset{\sim}{U}^{(1)}_{\ell m}(K_1,\vec{r}) + d_{\ell}\,m\,\frac{1}{K_1}\underset{\sim}{\nabla}\times\underset{\sim}{U}^{(1)}_{\ell m}(K_1,\vec{r})\right] \tag{34}$$

$$\underset{\sim}{B}_{in}(\underset{\sim}{r}) = -\frac{K_1}{\omega}\sum_{\ell=1}^{\infty}\sum_{m=\pm 1} mi^{\ell+1}\sqrt{\pi(2\ell+1)}\left[d_{\ell}\,\underset{\sim}{U}^{(1)}_{\ell m}(K_1,\vec{r}) + c_{\ell}\,m\,\frac{1}{K_2}\underset{\sim}{\nabla}\times\underset{\sim}{U}^{(1)}_{\ell m}(K_1,\vec{r})\right]$$

for $r < a$.

The boundary conditions are

$$\hat{e}_r \times (\underset{\sim}{E}_{out} + \underset{\sim}{E}_i) = \hat{e}_r \times \underset{\sim}{E}_{in} \quad , \tag{35}$$

$$\hat{e}_r \times (\underset{\sim}{B}_{out} + \underset{\sim}{B}_i) = \hat{e}_r \times \underset{\sim}{B}_{in} \quad . \tag{36}$$

This leads to two pairs of inhomogeneous equations for the expansion coefficient

$$\left.\begin{aligned} c_\ell\, j_\ell(N\rho) - a_\ell\, h_\ell^{(1)}(\rho) &= j_\ell(\rho) \\ c_\ell[N\rho j_\ell(N\rho)]' - a_\ell[\rho h_\ell^{(1)}(\rho)]' &= [\rho j_\ell(\rho)]' \end{aligned}\right\} \tag{37}$$

and

$$\left.\begin{aligned} Nd_\ell\, j_\ell(N\rho) - b_\ell\, h_\ell^{(1)}(\rho) &= j_\ell(\rho) \\ d_\ell[N\rho j_\ell(N\rho)]' + Nb_\ell[\rho h_\ell^{(1)}(\rho)]' &= N[\rho j_\ell(\rho)]' \end{aligned}\right\} \tag{38}$$

where $K_1 = NK_2$, $\rho = K_2 a$, $K_1 a = N\rho$. By solving Eq. (37) for a_ℓ and Eq. (38) for b_ℓ one finds the coefficients of the external field to be

$$a_\ell = -\left\{\frac{j_\ell(N\rho)[\rho j_\ell(\rho)]' - j_\ell(\rho)[N\rho j_\ell(N\rho)]'}{j_\ell(N\rho)[\rho h_\ell^{(1)}(\rho)]' - h_\ell^{(1)}(\rho)[N\rho j_\ell(N\rho)]'}\right\} \tag{39}$$

$$b_\ell = +\left\{\frac{j_\ell(\rho)[N\rho j_\ell(N\rho)]' - N^2 j_\ell(N\rho)[\rho j_\ell(\rho)]'}{h_\ell^{(1)}(\rho)[N\rho j_\ell(N\rho)]' - N^2 j_\ell(N\rho)[\rho h_\ell^{(1)}(\rho)]'}\right\} . \tag{40}$$

where the prime denotes differentiation with respect to the argument ρ or $N\rho$. The total field at any point outside the sphere is the sum of the incident and induced fields

$$\begin{aligned} \underset{\sim}{E}(\underset{\sim}{r}) &= \underset{\sim}{E}_i(\underset{\sim}{r}) + \underset{\sim}{E}_{out}(\underset{\sim}{r}) \\ \underset{\sim}{B}(\underset{\sim}{r}) &= \underset{\sim}{B}_i(\underset{\sim}{r}) + \underset{\sim}{B}_{out}(\underset{\sim}{r}) \ . \end{aligned} \tag{41}$$

The radial component of the total complex Poynting vector is

$$S_R^* = \frac{1}{2} E_0^2 \left[E_\theta B_\phi^* - E_\phi B_\theta^*\right] . \tag{42}$$

where E_0 is the amplitude of the field. By Eq. (41) S_R^* is

$$S_R^* = \frac{1}{2} E_0^2 \left[E_{i\theta} B_{i\phi}^* - E_{i\phi} B_{i\theta}^*\right] + \frac{1}{2} \left[E_{out\ \theta} B_{out\ \phi}^* - E_{out\ \phi} B_{out\ \phi}^*\right]$$

$$+ \frac{1}{2} \left[E_{i\theta} B_{out\ \phi}^* + E_{out\ \theta} B_{i\phi}^* - E_{i\phi} B_{out\ \theta}^* - E_{out\ \phi} B_{i\theta}^*\right] . \qquad (43)$$

If one considers a concentric spherical surface of radius R about the diffracting sphere, the real part of S_R^* integrated over the sphere is equal to the flow of energy across it. To simplify consider the external medium to be a perfect dielectric, $K_2 = \omega\sqrt{\varepsilon_2}$. If the diffracting sphere is also nonconducting the net flow across any surface enclosing the sphere must be zero. However, if energy is converted into heat within the sphere, the net flow is equal to the amount absorbed and is directed inward. The total energy absorbed by the sphere, W_a, is

$$W_a = - E_0^2 \, \mathrm{Re} \int_0^{2\pi} d\phi \int_0^{\pi} d\theta \; S_R^* \, r^2 \sin\theta \; . \qquad (44)$$

The second term on the right-hand side of Eq. (47) measures the outward flow of the scattered energy from the diffracting sphere and the total scattered energy is

$$W_s = \frac{1}{2} E_0^2 \, \mathrm{Re} \int_0^{2\pi} d\phi \int_0^{\pi} d\theta \; (E_{out\ \theta} B_{out\ \phi}^* - E_{out\ \phi} B_{out\ \theta}^*) \sin\theta . \qquad (45)$$

Likewise the third term of Eq. (47) must be equal in magnitude to the sum of the absorbed and scattered energies. So the total energy is

$$W_t = W_a + W_s = -\frac{1}{2} E_0^2 \, \mathrm{Re} \int_0^{\pi} d\theta \int_0^{2\pi} d\phi (E_{i\theta} B^*_{out\,\phi} + E_{out\,\theta} B^*_{i\phi} - E_{i\phi} B^*_{out\,\theta}$$

$$- E_{out\,\phi} B^*_{i\theta}) \sin\theta \, . \tag{46}$$

To calculate W_t we allow R to grow very large and introduce the asymptotic values

$$\left.\begin{aligned} j_\ell(\rho) &\simeq \frac{1}{\rho} \cos(\rho - \frac{\ell+1}{2}\pi) \\ h_\ell^{(1)}(\rho) &\simeq \frac{1}{\rho} (-i)^{\ell+1} e^{i\rho} \end{aligned}\right\} \tag{47}$$

into Eq. (32) and Eq. (33). The integrals can be evaluated with the help of the following two equations:

$$\int_0^{\pi} \left\{ \frac{dP_\ell^1}{d\theta} \frac{dP_\ell^1}{d\theta} + \frac{1}{\sin^2\theta} P_\ell^1 \right\} \sin\theta d\theta = \begin{cases} 0 \, , & \text{if } \ell \neq 1 \\ \dfrac{2}{2\ell+1} \dfrac{(\ell+1)!}{(\ell-1)!} (\ell(\ell+1)) & \text{if } \ell = 1 \end{cases} \tag{48}$$

$$\int_0^{\pi} \left\{ \frac{P_{\ell'}^1}{\sin\theta} \frac{dP_\ell^1}{d\theta} + \frac{P_\ell^1}{\sin\theta} \frac{dP_{\ell'}^1}{d\theta} \right\} \sin\theta d\theta = 0 \, . \tag{49}$$

So one can find that the total energy, W_t, is

$$W_t = \frac{\pi}{K_2^2} E_0^2 \sqrt{\varepsilon_2} \, \mathrm{Re} \sum_{\ell=1}^{\infty} (2\ell+1)(a_\ell + b_\ell) \, . \tag{50}$$

The total cross section of the sphere is defined as the ratio of the total energy per second to the energy density of the incident wave:

$$\sigma_t = \frac{2\pi}{K_2^2} \text{Re} \sum_{\ell=1}^{\infty} (2\ell+1)(a_\ell+b_\ell) \tag{51}$$

in $(\text{meters})^2$. By substituting Eq. (39) and Eq. (40) into Eq. (51) one can calculate the total cross section.

CHAPTER III

EXPERIMENT

In order to test Mie's theory of light scattering from metal spheres a way to make spheres of controlled sizes had to be found. Moreover, it is desirable not to have the strong influence of an external dielectric medium, an added complication. Lastly, the spheres should not be close to one another. The sample preparation technique below satisfies these requirements.

When a thin film of silver is heated on a surface it separates into a metal island film. These island particles of silver are oblate in shape like flattened spheres (Figure 1). If the contact area between the substrate and the silver is reduced then the surface tension of the silver at room temperature and above will dominate over the attractive force between the silver and the substrate. Thus, the particles will tend to be more spherical. The substrate that allows this was developed by the Submicron Physics Group at the Oak Ridge National Laboratory by M. Buncick et al. [28]. The surprising mobility of silver films well below the melting point of bulk silver is called "surface melting," a phenomenon useful in this case.

To make this substrate (given the name posts) one must start with a clean quartz slide. The slide is carefully cleaned using detergent, and then rinsed in distilled water, followed by ultrasonic cleaning in acetone and then in methanol. The slide is then dried using nitrogen gas. After cleaning the slide one must be careful not

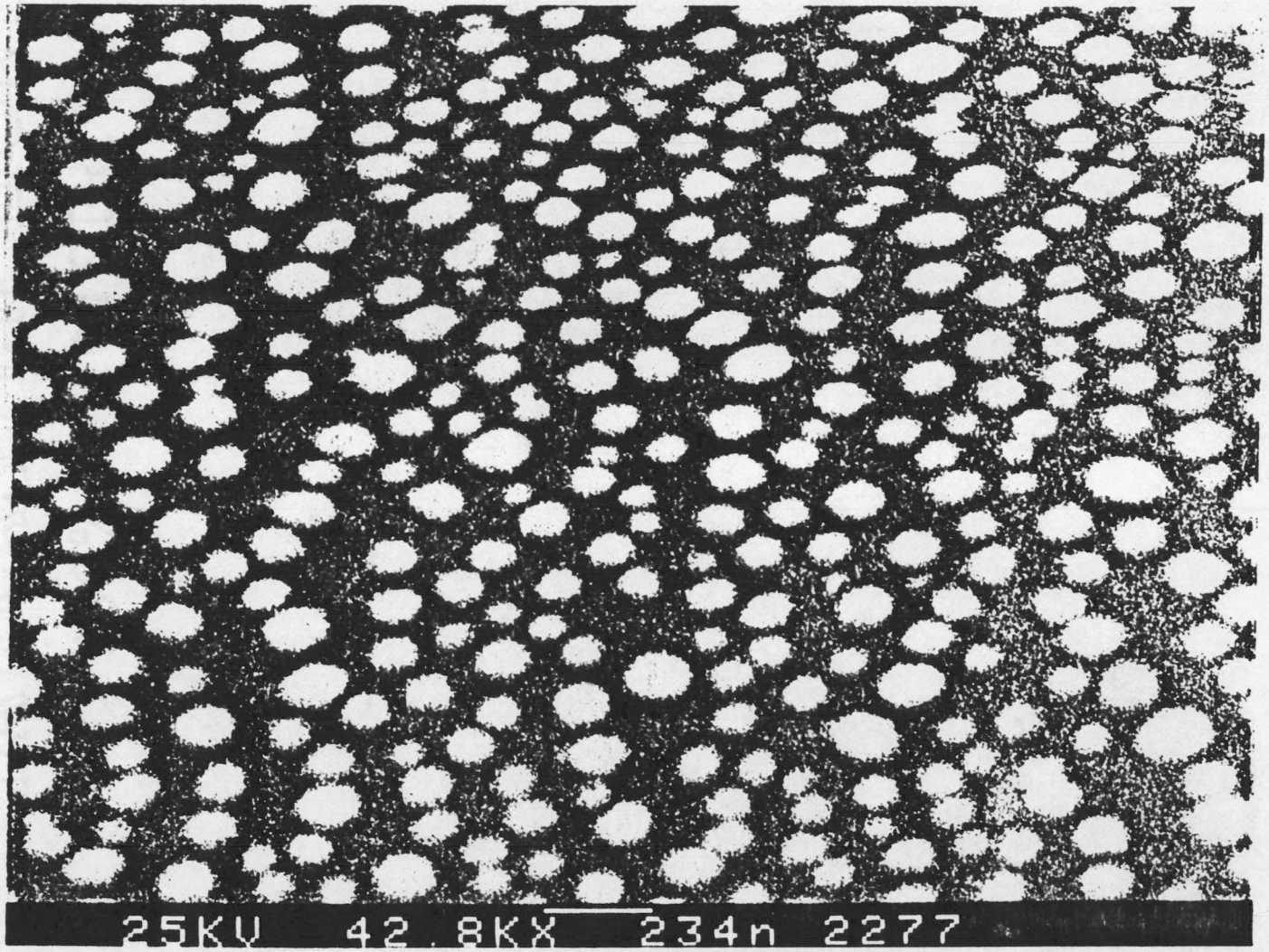


Figure 1. Silver metal island film at an angle of 50°.

to touch it or place it on anything that has not been cleaned in a like manner. (The quartz surface must be clean to get good bonding between the substrate and the additional quartz that is to be evaporated onto the slide.) After cleaning, the slide is placed in an electron-beam thin-film evaporator. A mechanical, sorption, and cryopump system is used to obtain the vacuum. This system is used instead of a mechanical and diffusion pump system for two reasons: (1) a better vacuum in a shorter amount of time can be obtained, and (2) since the diffusion pump requires vacuum oil, and the cryopump does not, the samples are not contaminated with oil.

Silicon dioxide is evaporated first onto the quartz slide (silicon dioxide is used for the substrate because it is transparent in the optical region 300 nm to 600 nm, which is the region of interest). Evaporated silicon dioxide is used to form the posts instead of just using the quartz slide (which is made of fused quartz) because evaporated silicon dioxide etches at a much faster rate (up to ten times) than fused silicon dioxide. After reaching a base pressure of 8×10^{-7} Torr, a 500 nm layer of silicon dioxide is evaporated on the sample at a rate of 0.5-1.0 nm/s. This layer serves as the substrate into which submicron posts will be etched. If the pressure goes above 3×10^{-6} Torr during the evaporation it is considered best to cease the evaporation and let the pressure go back to 8×10^{-7} Torr. The low pressure is needed to insure that the silicon dioxide evaporates evenly and that a minimum number of gas molecules are trapped inside the film (traces of gas molecules could result in

the cracking of the silicon dioxide film). Also, too rapid a rate of evaporation can result in the cracking of the silicon dioxide film.

In order to make posts that are uniform in size and widely separated, Dow latex spheres [29] are used as a mask. Mosaic arrays of spherical latex particles are formed by using a spin coating process [30]. A monolayer can be formed (Figure 2) if the latex spheres flow across the substrate at high shear rates while the excess material is dispelled. The latex spheres must completely wet the substrate, and the spin speed must be optimized. If the spin speed is too low a multilayer will be formed; if the spin speed is too high voids will occur in the monolayer. The coating is prepared by flooding a clean quartz slide with polystyrene latex containing 10% solids (spheres each having a diameter of 482 nm) and spinning at 3000 rpm until the coating is dry. The spin time is typically brief, being roughly 30 sec.

After a monolayer of latex spheres is achieved the sample is coated at normal incidence with 10 nm of silver, again using the e-beam thin film evaporator. The pressure for the silver evaporation should be below 2×10^{-6} Torr and the rate of evaporation should be about 1 nm/s. Silver is deposited in this way upon the latex spheres, but silver is also deposited in triangular patches between the spheres. The portions of silicon dioxide surface which are exposed to the evaporation beam in the gap between the nearly closed-packed spheres thus receives a silver overlayer. These triangular patches of silver form a semi-ordered, hexagonal array which is broken in only

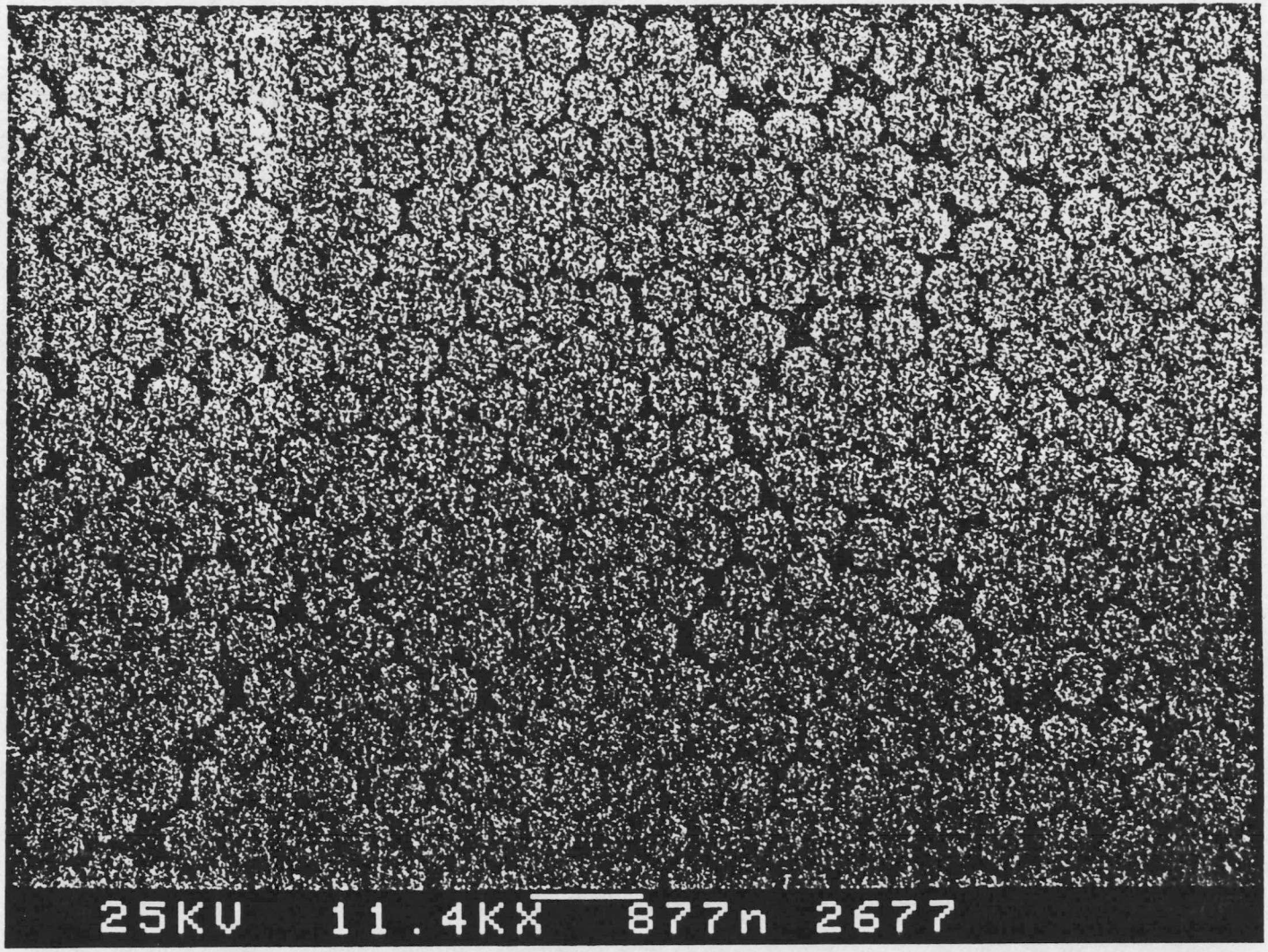


Figure 2. Monolayer of latex sphere with diameter of 482 nm.

a few areas due to the difficulty in achieving a perfectly close-packed monolayer of latex spheres. The latex spheres are now removed by immersing the sample in dichloromethane in an ultrasonic cleaner. This leaves the array of triangular patches exposed. After a few minutes the sample is removed from the cleaner, rinsed with methanol, and then blown dry with nitrogen gas. Next, the samples are heat treated in a convection oven at 750°C for one minute in order to change the triangular patches into spheroidal particles. The heat treatment is of a short enough duration that there is little migration of the particles. Thus, the etch mask consists of silver spheroids arranged in a semi-ordered, hexagonal array (Figure 3).

Posts are formed in the silicon dioxide by placing a sample in a reactive ion etching system using CHF_3 as the reactive species. Power settings of 50 W forward and 35 W reflected were used and an etching pressure of 5 microns for the CHF_3 gas was found to produce an etching rate of 10 nm/min in the silicon dioxide. The sample is etched for twenty-five minutes to produce posts that are about 250 nm tall (Figure 4). Since we use an etch mask that is produced using the latex spheres, the posts are all approximately the same size (to insure a small distribution of the sizes of the spheres). They are widely separated (to allow enough room for the spheres to be increased in size and so that the theory for isolated spheres applies). If the distribution of sizes of the mask particles is too broad, one ends with a broad distribution of post sizes. This in turn leads to a large distribution of sphere sizes, which smears the absorbance spectrum.

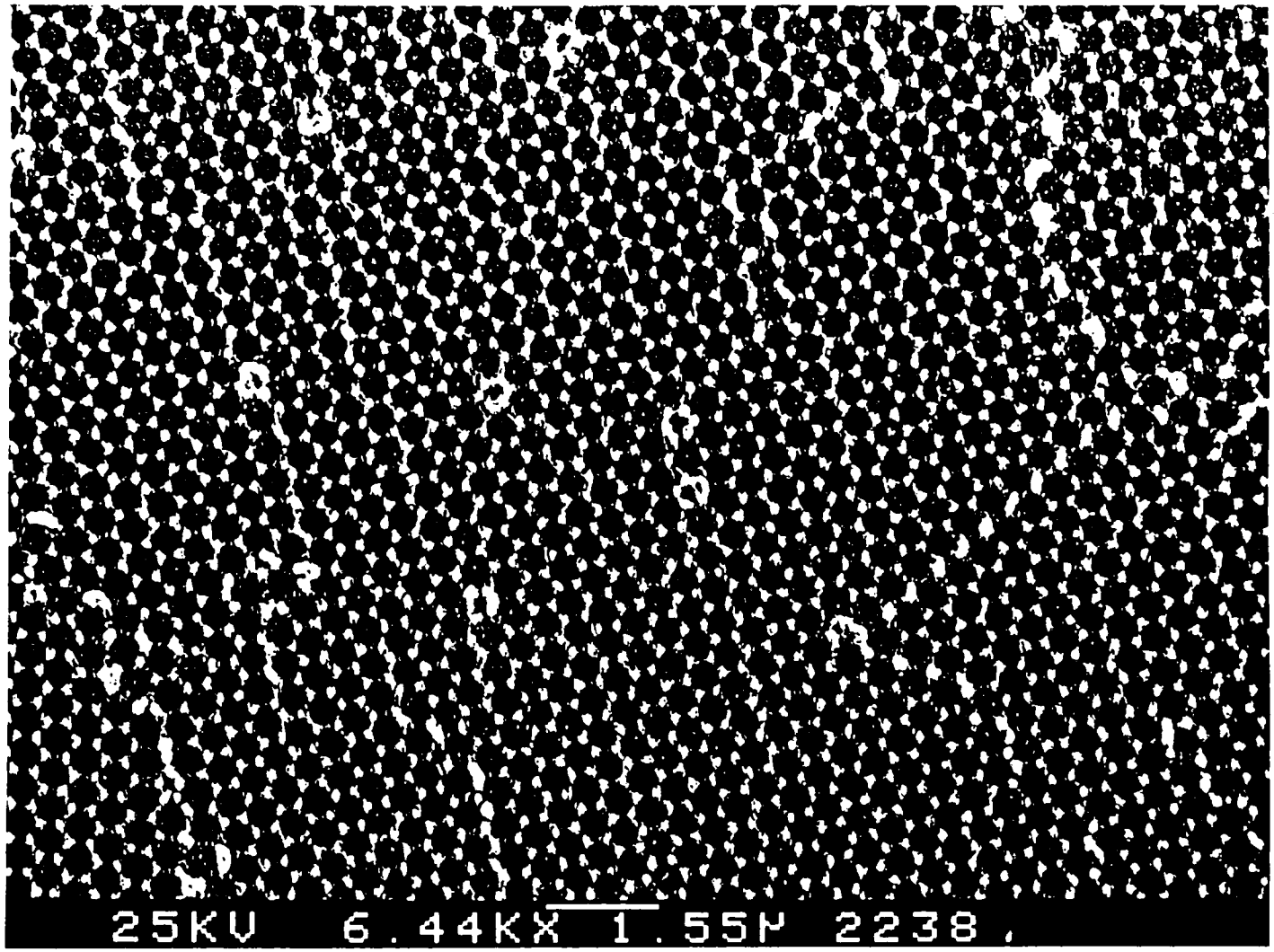


Figure 3. Etch mask of silver spheroids arranged in a semi-ordered, hexagonal array.

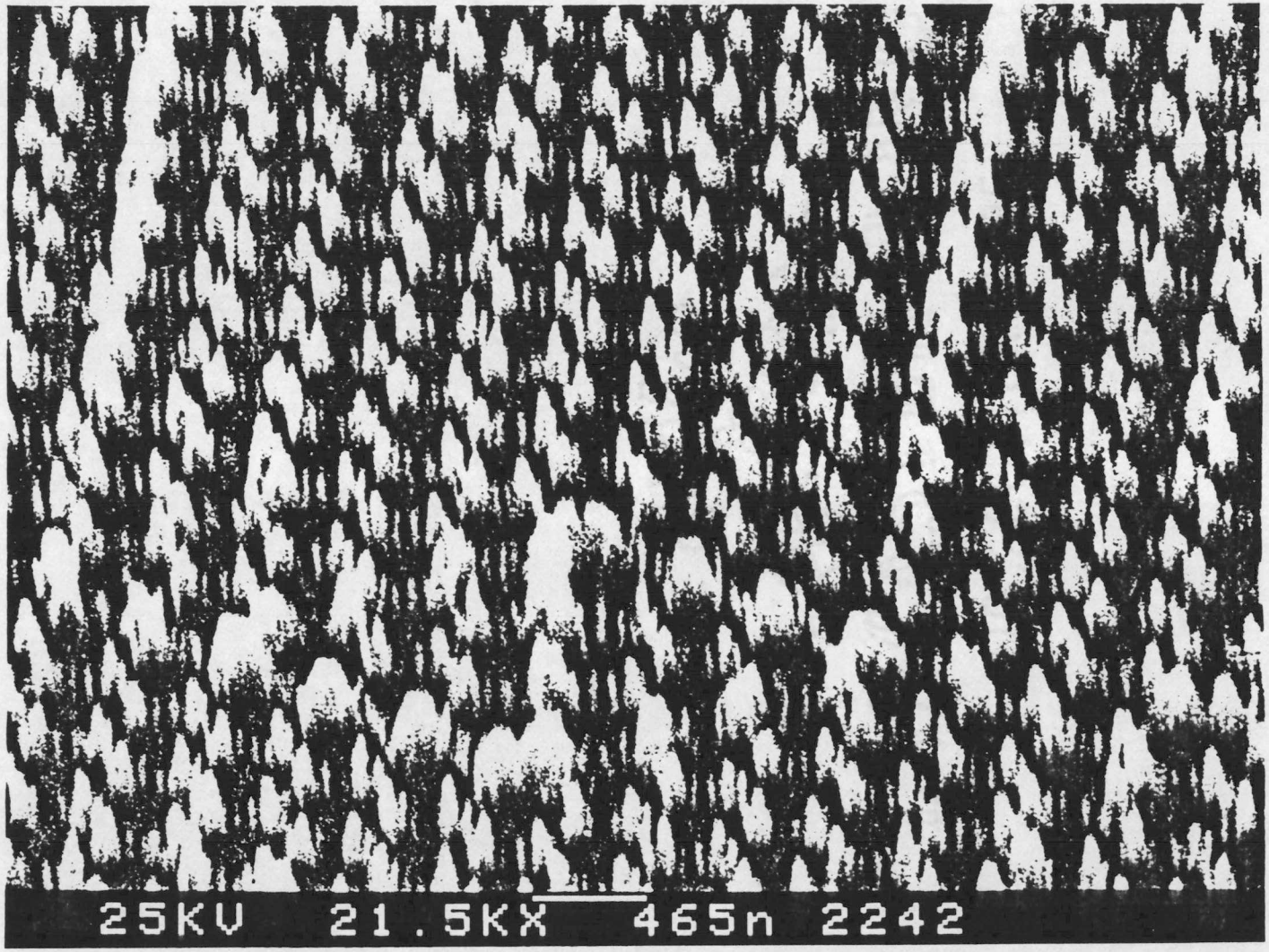


Figure 4. Silicon dioxide posts at an angle of 50°.

The silver spheres are formed by evaporating silver onto the posts. To be sure that the silver is evaporated only on the tips of the posts (and not in between where small particles can be formed) an angle of incidence of 80 with respect to the normal is used. Also, the height of the posts must be above 200 nm to insure that the silver is primarily placed on the tips of the posts. The sample is rotated during evaporation to ensure even deposition on the posts. Each post is thus covered with silver on the tip.

After the post substrate is coated with silver the sample is heated at 750°C for one minute (Figure 5). The high temperature is used because it gives the best sphere shape. Lower temperatures were tried, but the resulting particles were not spherical. The time duration of one minute was found to optimize the spherical shape. Heat treatment for a longer period of time was found to lead to anomalous data. The anomalies are thought to be due to a sulfide layer on the outside of the sphere. If for some reason (say for reproduction purposes) a longer time is needed, it is best to use an oven in which an inert gas floods the chamber. The gas acts to inhibit formation of the sulfide layer.

After heating, the spheres are placed in a spectrophotometer and an absorbance spectrum is taken in the range from 300 nm to 600 nm. Polarized light is used, and a spectrum of both P and S polarization is taken. The silver spheres are then removed and a larger amount of silver is evaporated to form larger spheres. By evaporating an ever increasing amount of silver (using the same substrate each time) and

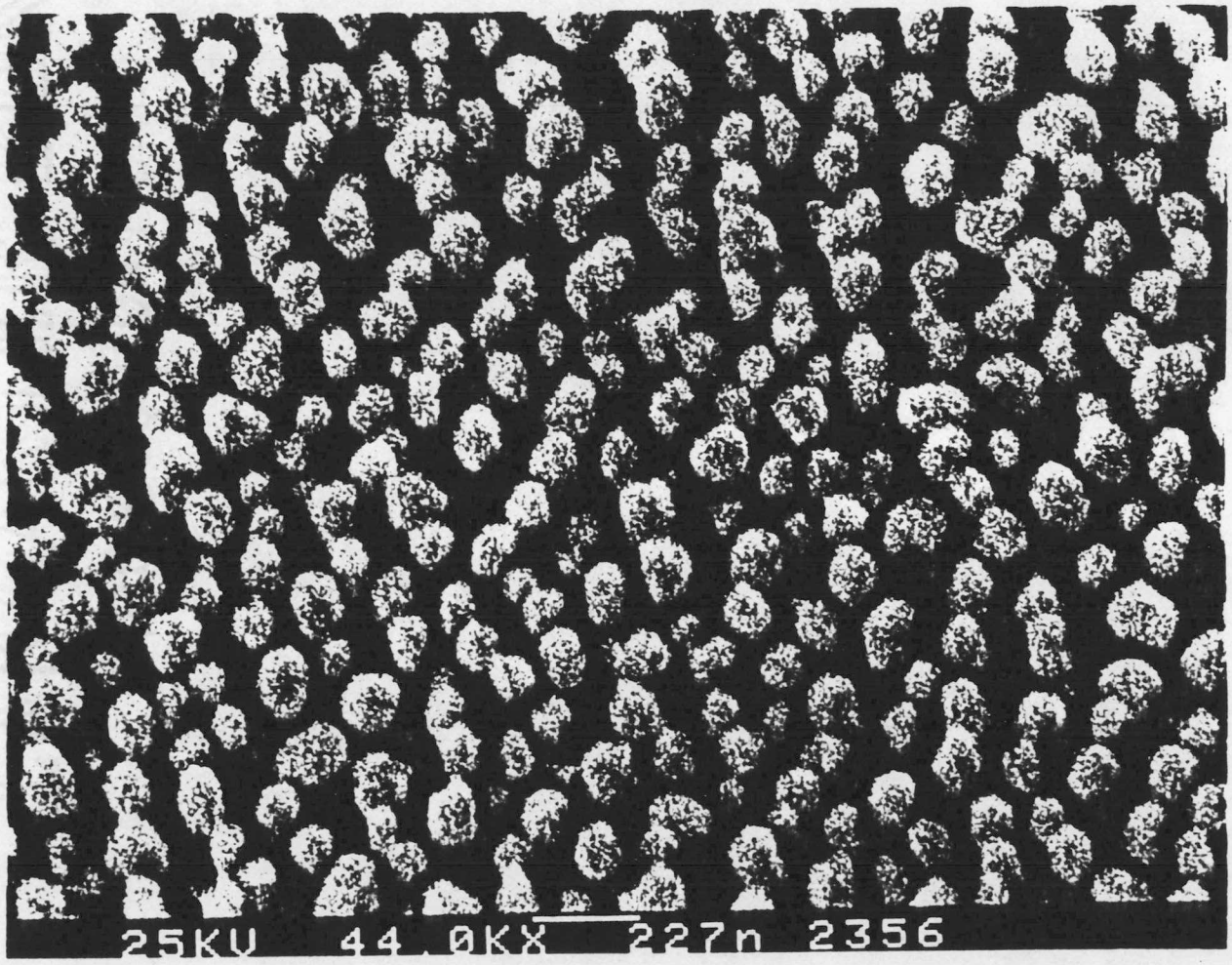


Figure 5. Silver spheres on quartz posts.

heat treating the sample, a systematic determination of sphere sizes and absorbance peak data are obtained. Samples with radii ranging from 40 nm to 70 nm were used in this work. By using a scanning electron microscope, electron micrographs can be obtained from which the size of the spheres and the size distribution can be determined.

CHAPTER IV

RESULTS AND ANALYSIS

Before presenting the experimental results, we first briefly review the theory of the scattering of electromagnetic waves by an absorbing sphere. From the Mie theory, one can show that the total cross section for this case is given by

$$\sigma_t = \frac{2}{K^2} \text{Re} \sum_{\ell=1}^{\infty} (2\ell+1)(a_\ell + b_\ell) \tag{51}$$

where K is the magnitude of the wave vector of the incident electromagnetic wave, and Re means that one takes the real part of the expression. The quantities a_ℓ and b_ℓ are coefficients that are used on the multipole expansions of the scattered electric and magnetic fields, and which can be determined from the vector boundary conditions on the fields at the surface of the spherical particle as in Eq. 4.53 in Bohern and Huffman [31,32]. In the experiment, the measured quantity is the optical absorbance which can be related to the total cross section by

$$A = \log_{10} \left(\frac{1}{1-N\sigma_t}\right) \tag{52}$$

where N is the number of spherical scatterers per unit area on the substrate [33]. The spheres were sufficiently far apart so that the individual cross sections combine incoherently.

The measured and calculated absorbance at normal incidence to the surface plane are presented in Figures 6 through 11 as a function of wavelength for several different sphere radii. The experimental data has been automatically corrected by the spectrophotometer to account for absorbance due to the quartz post substrate. The theoretical curves, as shown, were separately fit to the experimental curves by determining the value of N in Eq. (56) that would make the calculated absorbance approximately match one of the experimental peaks for each of the cases shown. Each value of N was later found to agree within 20% with the density of spheres on the substrate as determined by electron micrographs. The value of the sphere radius that was used in the calculations was slightly different from the experimental average sphere radius determined from the micrographs, but it is still within the experimental error for the average radius. The standard deviation of the sphere size on the samples was 12 nm. The values of the dielectric function, which were used in the calculations, were interpolated from data obtained from bulk optical measurements made on silver [34].

As seen in Figures 6 through 11, an increase in the sphere radius leads to the emergence of a second peak which begins to be resolved for sizes larger than about 55.5 nm. Increasing the radius further not only causes a diminution of the ℓ=1 peak relative to the ℓ=2,3 ... (mostly ℓ=2) peak, but also causes an increasing separation of the two peaks. While the experimental and calculated curves do not overlap perfectly, this is thought to be due to the small distribution

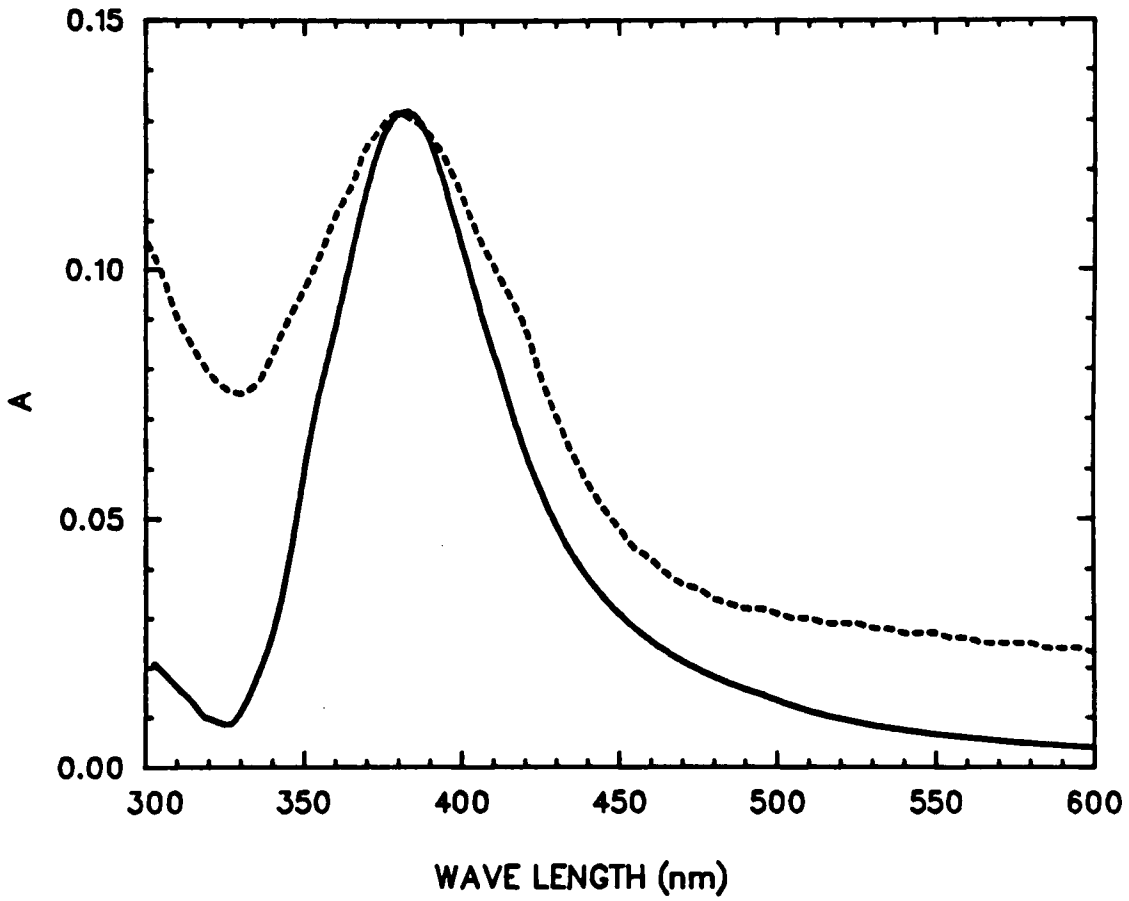


Figure 6. Absorbance spectrum of silver spheres, r = 40.0 nm.

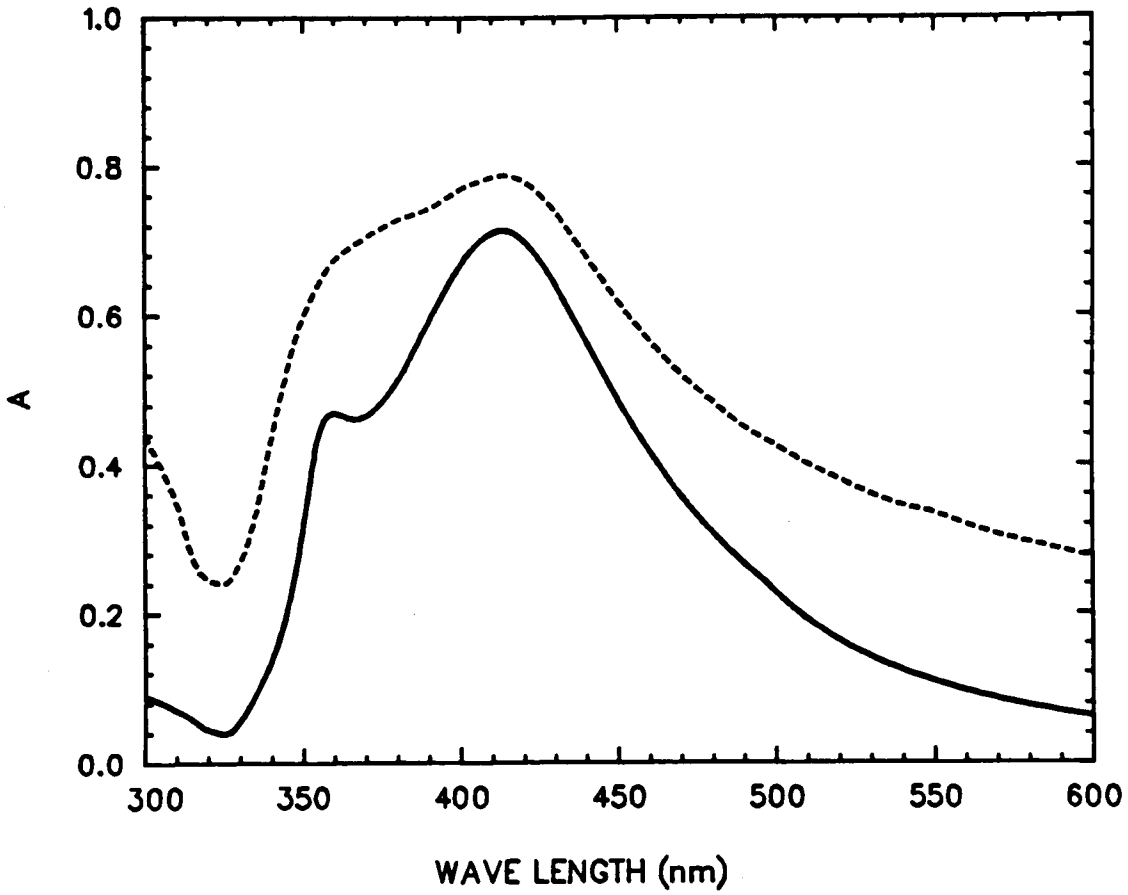


Figure 7. Absorbance spectrum of silver spheres, r = 55.5 nm.

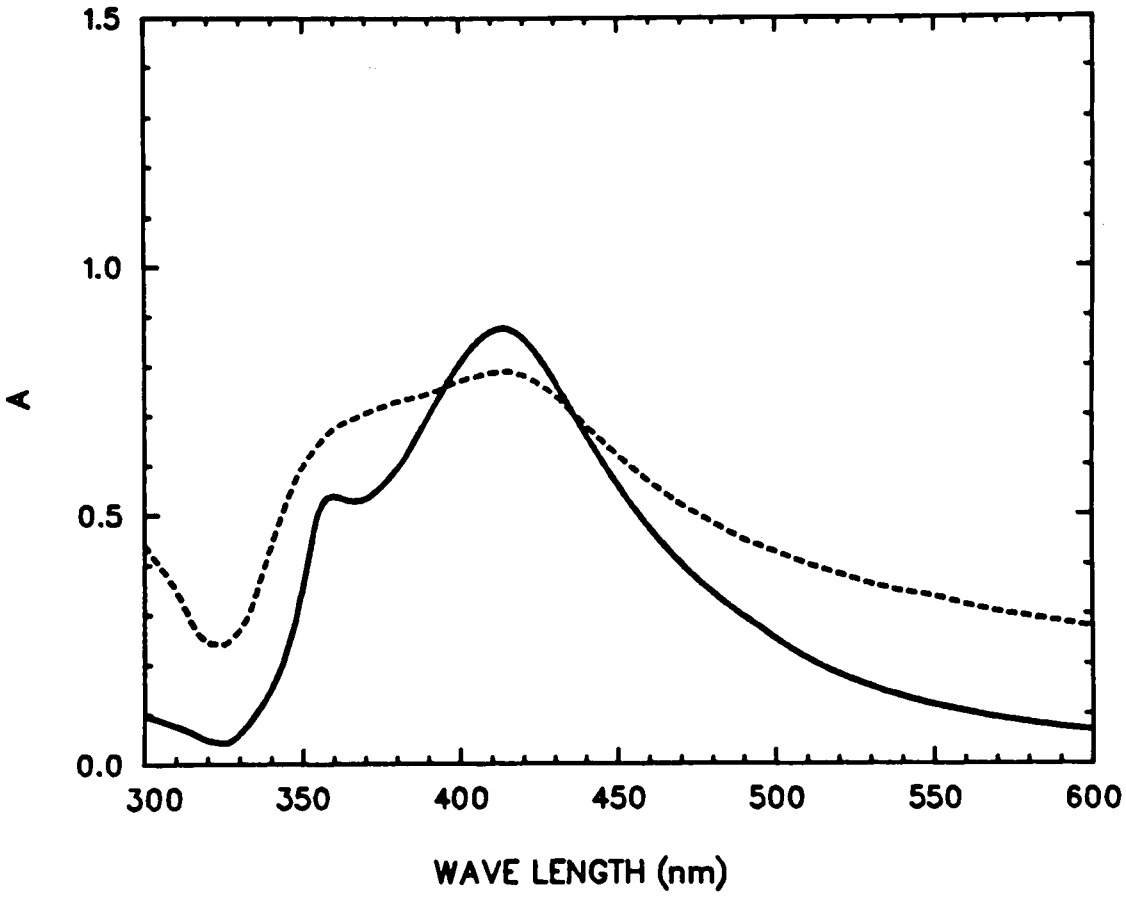


Figure 8. Absorbance spectrum of silver spheres, r = 59.0 nm.

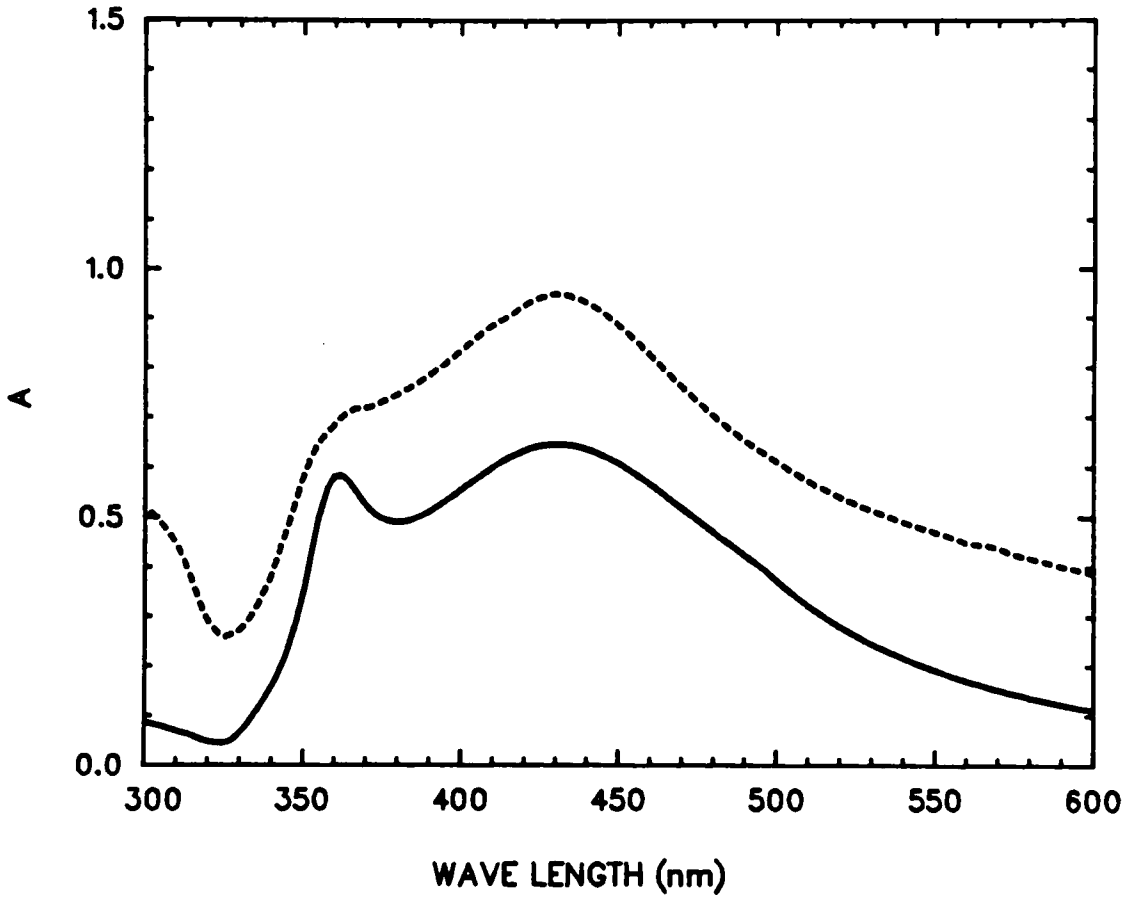


Figure 9. Absorbance spectrum of silver spheres, r = 62.0 nm.

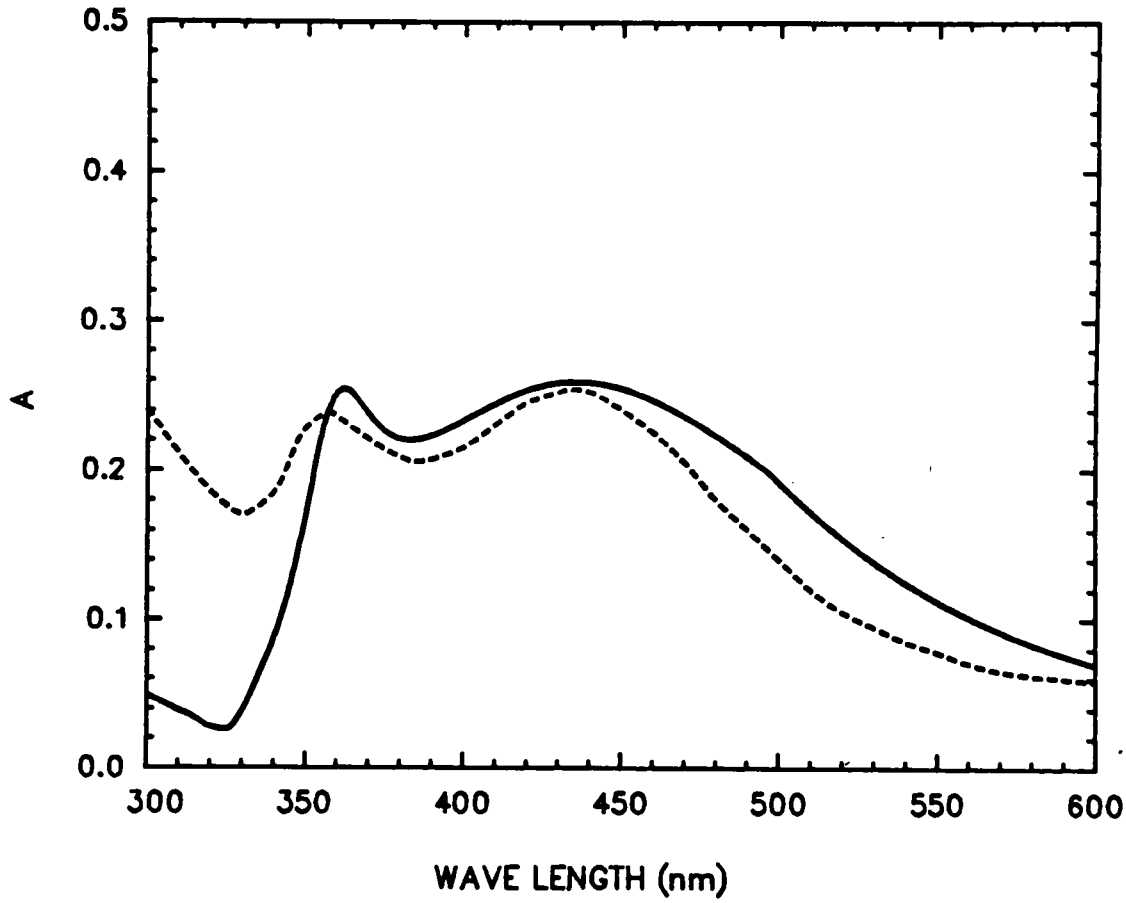


Figure 10. Absorbance spectrum of silver spheres, r = 63.5 nm.

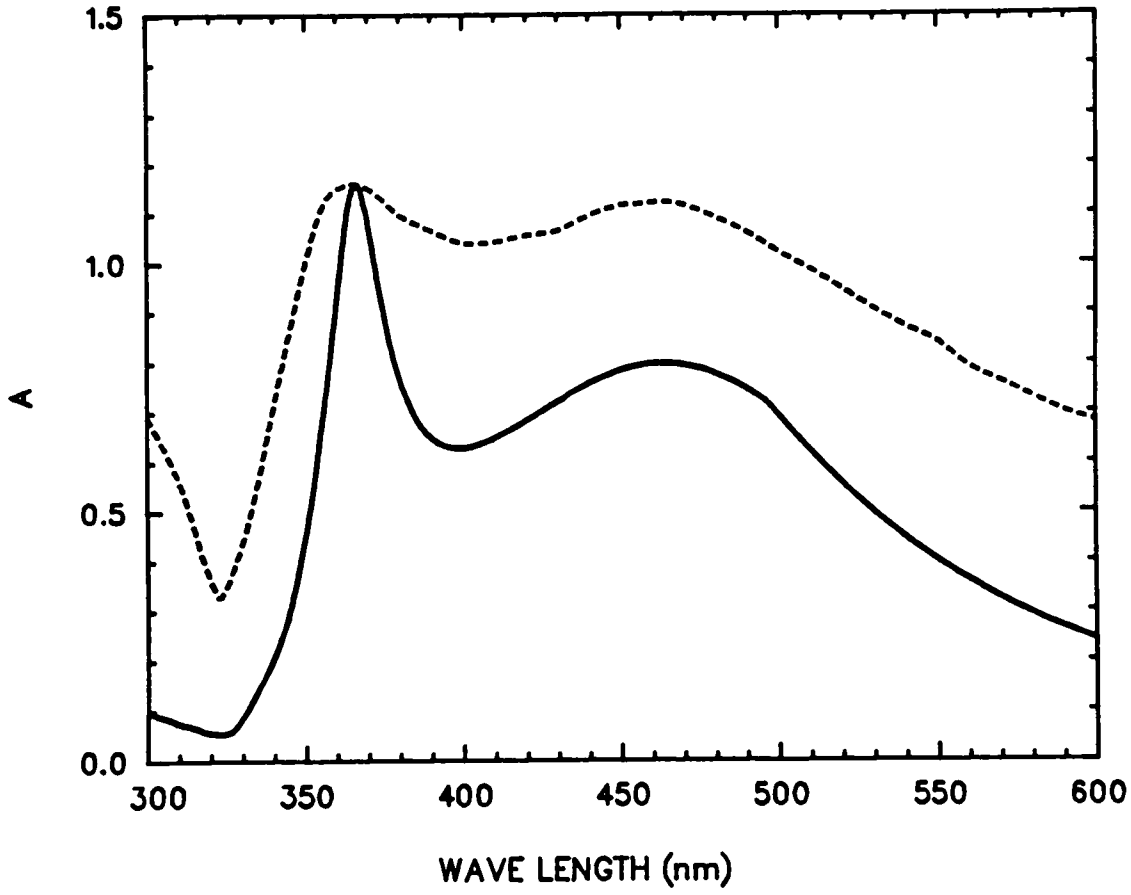


Figure 11. Absorbance spectrum of silver spheres, r = 70 nm.

of sphere sizes in the samples and the response time of the spectrophotometer. Nevertheless, there is good agreement between experiment and the Mie theory in the overall shape of the absorbance spectra and in the positions of the peaks. In Figure 12 the contributions of the dipole through octupole modes are shown calculated from theory. As can be seen by taking only the dipole mode into consideration, only one resonance is observed. With the dipole and quadrupole contributions, two modes are observed. Octupole and higher order modes contribute little to the overall structure for these spheres.

In Figure 13, the position of the experimental and calculated ℓ=1,2 peaks are plotted against the average sphere radius. The agreement between theory and experiment is sufficient over the range of the experimental data to permit one to state that deviations from the Mie theory are not found. In Tables 1 and 2, theoretical and experimental data are shown.

In Figure 14, the absorbance peak of a sample of spheres with radii ranging from 15 nm to 35 nm is shown. The sample was prepared in such a way that the spheres were not uniform in size so a smearing of the absorbance peak is observed. This shows clearly that one must have spheres that are uniform in size to obtain correct data.

Martinos has predicted peaks in the absorbance at energies higher than the bulk plasmon energy. We observe no such peaks. The sign error in one of the Mie coefficients in the textbook by Stratton [20] is repeated in the Martinos paper.

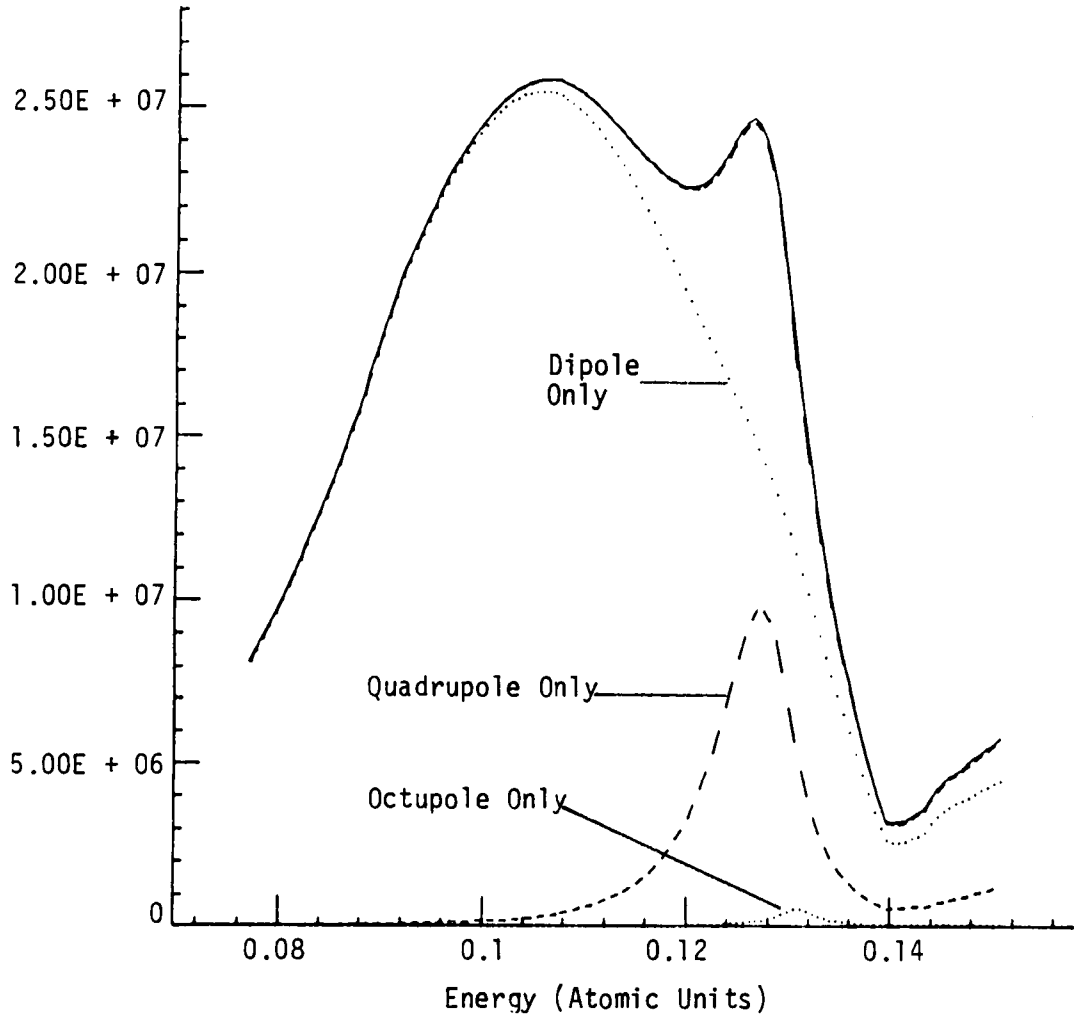


Figure 12. Contribution to the absorbance peak for dipole through octupole modes.

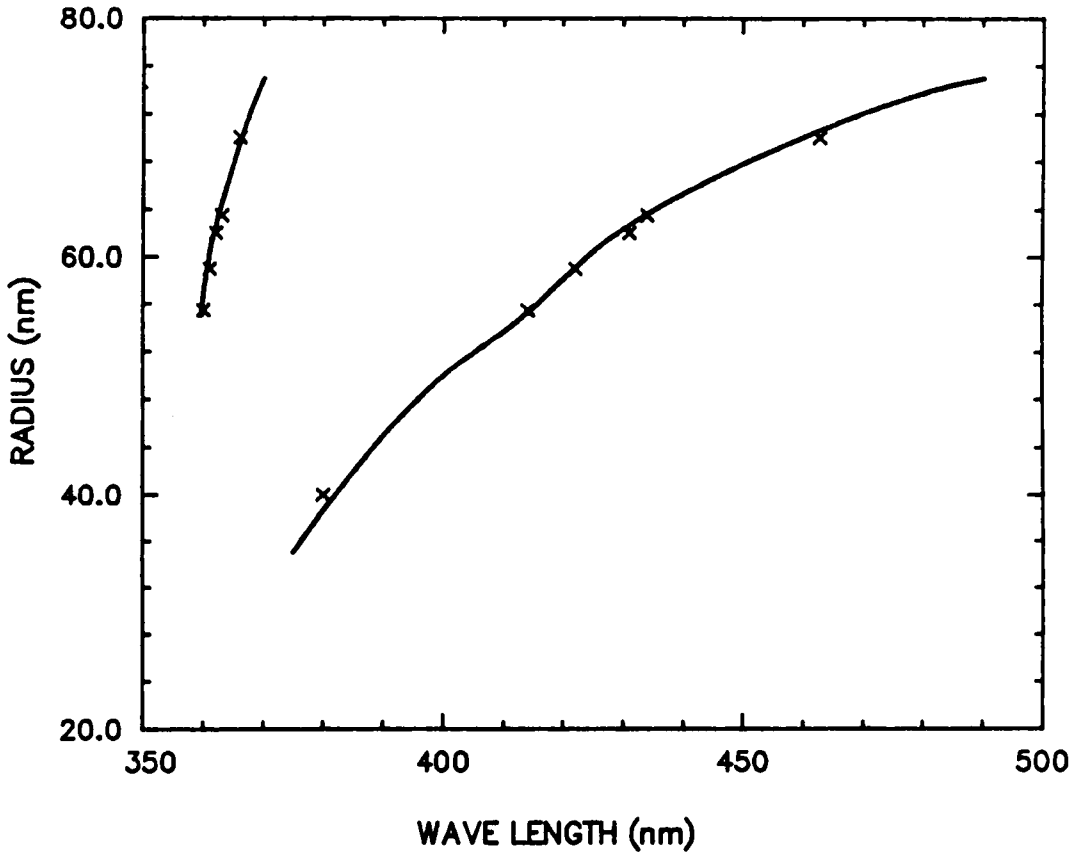


Figure 13. Retardation curve for the absorbance peaks of silver.

TABLE 1

THEORETICAL DATA

Radius (nm)	Wavelength (nm)(n=1)	Wavelength (nm)(n=2,...)
35.0	375.0	--
40.0	382.0	--
45.0	390.0	--
50.0	400.0	--
55.0	413.3	359.6
60.0	423.9	360.9
75.0	490.2	370.0

TABLE 2

EXPERIMENTAL DATA

Radius (nm)	Wavelength (nm)(n=1)	Wavelength (nm)(n=2,...)
40.0	380.0	--
55.5	414.0	360.0
59.0	422.0	361.0
62.0	431.0	362.0
63.5	434.0	363.0
70.0	462.8	366.0

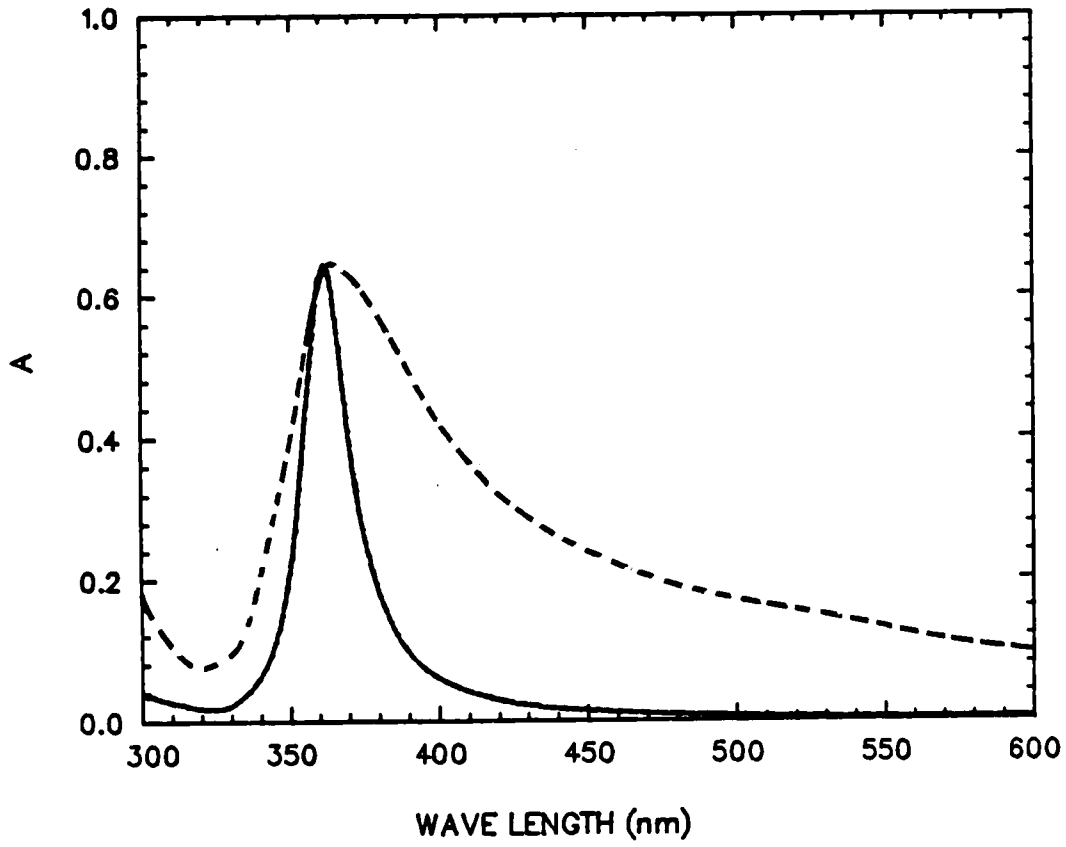


Figure 14. Absorbance peak of spheres with 15 nm $\leq$ r $\leq$ 35 nm.

CHAPTER V

CONCLUSION

We have discussed Mie's scattering theory of a sphere and have described a new technique for producing spherical particles for testing that theory. The particle radius could be controlled closely so that optical absorbance data could be compared well with a single particle model. Sizes range from 40 nm, where the dipole mode of oscillation dominates, to 70 nm, where higher order modes are apparent and retardation significantly shifts the resonances. Good agreement between the Mie theory and experimental data was obtained.

REFERENCES

REFERENCES

1. G. Mie, Ann. Phys. 25, 377 (1908).

2. G. Hawley, Small Wonder: Story of Colloids, Alfred A. Knopf, New York, 1947.

3. The Encyclopedia of Physics, Robert M. Besançon, Ed., Reinhold Publishing Co., New York (1966).

4. J. Rayleigh, Scientific Papers, Dover Publications, Inc., New York (1964).

5. A. Einstein, "Investigation of the Theory of the Brownian Motion," A. D. Cowper, Translator, Dover Publications, Inc., New York (1956).

6. P. Debye and E. Huckel, Phys. Zeits 24, 185, 305 (1923).

7. T. Svedberg and H. Rinde, J. Am. Chem. Soc. 46, 2677 (1924).

8. T. Zsigmondy, Ann. d. Physik 10, 1 (1902).

9. E. Ruska and M. Knoll, Ann. d. Physik 12, 607, 641 (1932).

10. S. Martinos, Phys. Rev. B 31, No. 4, 2029 (1985).

11. R. Ruppin, Phys. Rev. B 11, No. 8, 2871 (1975).

12. A. D. Boardman and B. V. Paranjape, J. Phys. F 7, No. 9, 1935 (1977).

13. G. Grehan and G. Gouesbet, Appl. Opt. 23, No. 24, 4462 (1984).

14. D. D. Evans, Appl. Opt. 13, No. 7, 1545 (1974).

15. R. M. Drake and J. E. Gordon, Am. J. Phys. 53, No. 10, 955 (1985).

16. C. Bar-Isaac and A. Hardy, Am. J. Phys. 43, No. 3, 275 (1975).

17. D. B. Vafin and A. F. Dregalin, Inzhenerno-Fizicheskii Zhurnal 35, No. 4, 648 (1978).

18. J. E. Gordon, J. Opt. Soc. Am. A 2, No. 2, 156 (1985).

19. J.-D. Ganiere, R. Rechsteiner, and M.-A. Smithard, Solid State Commun. 16, 113 (1975).

20. M.-A. Smithard, Solid State Commun. 13, 153 (1973).

21. A. Kawakata and R. Kubo, J. Phys. Soc. Japan 21, No. 9, 1765 (1966).

22. M. Kerker, O. Siiman, L. A. Bumm, and D.-S. Wang, Appl. Opt. 19, 3253 (1980).

23. M. Kerker and S. D. Druger, Appl. Opt. 18, No. 8, 1172 (1979).

24. D.-S. Wang, H. Chen, and M. Kerker, Appl. Opt. 19, No. 14, 2256 (1980).

25. B. J. Messinger, K. U. von Ruben, R. K. Chang, and P. W. Barber, Phys. Rev. B 24, No. 2, 649 (1981).

26. J. D. Jackson, Electrodynamics, 2nd edition, Chap. 16, Wiley, New York, 1975.

27. J. A. Stratton, Electromagnetic Theory, Chap. 9, McGraw-Hill, New York, 1941.

28. M. C. Buncick, R. J. Warmack, and T. L. Ferrell, Am. Phys. Soc. 30, No. 10, 1783 (1985).

29. Dow Latex Particles, Duke Scientific, Palo Alto, California.

30. H. W. Deckman and J. H. Dunsmuir, Appl. Phys. Lett. 41, 4 (1982).

31. C. F. Bohren and D. R. Huffman, Absorption and Scattering of Light by Small Particles, Chap. 4, Wiley, New York, 1983.

32. During the research, a sign error for b_ℓ was discovered in Eq. 9.25.11 in Stratton (Ref. 20). The minus sign to the right of the equals symbol in that equation should actually be a plus sign. Not using the correct sign was found to have a marked effect on the calculated theoretical cross section.

33. S. W. Kennerly, J. W. Little, R. J. Warmack, and T. L. Ferrell, Phys. Rev. B 29, No. 6, 2926 (1984).

34. H. J. Hagemann, W. Gudat, and C. Kuntz, Deutsches Elektronen-Synchrotron Report No. DES4-SR-7417 (unpublished).

APPENDICES

APPENDIX A

SPHERICAL BESSEL FUNCTIONS

Series Expansions

$$J_{\ell+\frac{1}{2}}(x) = \left(\frac{x}{2}\right)^{\ell-\frac{1}{2}} \sum_{j=0}^{\infty} \frac{(-1)^j}{j!\ \Gamma\left(j-\left(\ell+\frac{1}{2}\right)+1\right)} \left(\frac{x}{2}\right)^{2j} \tag{A.1}$$

$$J_{-\left(\ell-\frac{1}{2}\right)}(x) = \left(\frac{x}{2}\right)^{-\left(\ell+\frac{1}{2}\right)} \sum_{j=0}^{\infty} \frac{(-1)^j}{j!\ \Gamma\left(j-\left(\ell+\frac{1}{2}\right)+1\right)} \left(\frac{x}{2}\right)^{2j} \tag{A.2}$$

$$N_{\ell+\frac{1}{2}}(x) = \frac{J_{\ell+\frac{1}{2}}(x)\cos\left(\ell+\frac{1}{2}\right)\pi - J_{-\left(\ell+\frac{1}{2}\right)}(x)}{\sin\left(\ell+\frac{1}{2}\right)\pi} \tag{A.3}$$

Spherical Bessel Functions

$$j_\ell(x) = (-x)^\ell \left(\frac{1}{x}\frac{d}{dx}\right)^\ell \left(\frac{\sin x}{x}\right) \tag{A.4}$$

$$n_\ell(x) = (-x)^\ell \left(\frac{1}{x}\frac{d}{dx}\right)^\ell \left(\frac{\cos x}{x}\right) \tag{A.5}$$

Small Argument Limit of Spherical Bessel Functions $x \ll 1, \ell$

$$j_\ell(x) \to \frac{x^\ell}{(2\ell+1)!!}\left(1 - \frac{x^2}{2(2\ell+3)} + \ldots\right) \tag{A.6}$$

$$n_\ell(x) \to \frac{(2\Pi+1)!!}{x}\left(1 - \frac{x^2}{2(1-2\ell)} + \ldots\right) \tag{A.7}$$

where

$$(2\ell+1)!! = (2\ell+1)(2\ell-1)(2\ell-3)\ \ldots\ (5)\cdot(3)\cdot(1) \tag{A.8}$$

Large Argument Limits $x \gg \ell$

$$j_\ell(x) \to \frac{1}{x}\sin\left(x - \frac{\ell\pi}{2}\right) \tag{A.9}$$

$$n_\ell(x) \to \frac{1}{x}\cos\left(x - \frac{\ell\pi}{2}\right) \tag{A.10}$$

$$h_\ell^{(1)}(x) \to (-i)^{\ell-1}\,\frac{e^{ix}}{x} \tag{A.11}$$

APPENDIX B

ANGULAR MOMENTUM OPERATOR

$$
\left.
\begin{aligned}
L &= L_x + L_y + L_z \\
L^2 &= L_x^2 + L_y^2 + L_z^2 \\
L_x &= \frac{1}{i}\left(-\sin\phi \frac{\partial}{\partial\theta} - \cot\theta \cos\phi \frac{\partial}{\partial\phi}\right) \\
L_y &= \frac{1}{i}\left(\cos\phi \frac{\partial}{\partial\theta} - \cot\theta \sin\phi \frac{\partial}{\partial\phi}\right) \\
L_z &= \frac{1}{i}\frac{\partial}{\partial\phi} \\
L^2 &= -\left[\frac{1}{\sin\theta}\frac{\partial}{\partial\theta}\left(\sin\theta \frac{\partial}{\partial\theta}\right) + \frac{1}{\sin^2\theta}\frac{2}{\partial\phi^2}\right] \\
L_+ &= (L_x + iL_y) \\
L_- &= (L_x - iL_y)
\end{aligned}
\right\} \qquad \text{(B.1)}
$$

Operator Equations

$$\left.\begin{aligned}
&[L_x, L_y] = i\, L_z \\
&[L_z, L^2] = 0 \\
&[L_x, L_y] = i\, L_z \\
&[L_y, L_z] = i\, L_x \\
&[L_z, L_x] = i\, L_y \\
&[L_z, \underset{\sim}{L}] = 0 \\
&L^2\, \underset{\sim}{L} = \underset{\sim}{L}\, L^2 \\
&\underset{\sim}{L} \times \underset{\sim}{L} = i\, \underset{\sim}{L} \\
&L_j\, \nabla^2 = \nabla^2\, L_j
\end{aligned}\right\} \qquad (B.2)$$

where

$$\nabla^2 = \frac{1}{r} \frac{\partial^2}{\partial r^2} (r) - \frac{L^2}{r^2} \qquad (B.3)$$

$$\begin{aligned}
&L_+\, Y_{\ell m}(\theta,\phi) = \sqrt{(\ell-m)(\ell+1+m)}\; Y_{\ell,m+1}(\theta,\phi) \\
&L_-\, Y_{\ell m}(\theta,\phi) = \sqrt{(\ell+m)(\ell+1-m)}\; Y_{\ell,m-1}(\theta,\phi) \\
&L_-\, L = L_x^2 + L_y^2 + L_z = L^2 - L_z^2 + L_z \\
&L_z\, Y_{\ell m}(\theta,\phi) = m\, Y_{\ell m}(\theta,\phi)
\end{aligned} \qquad (B.4)$$

where $Y_{\ell m}(\theta,\phi)$ is the spherical harmonics

$$\left.\begin{aligned} L^2\, Y_{\ell m}(\theta,\phi) &= \ell(\ell+1)\, Y_{\ell m}(\theta,\phi) \\ Y_{\ell m}(\theta,\phi) &= (-1)^m \sqrt{\frac{(2\ell+1)}{4\pi}\frac{(\ell-m)!}{(\ell+m)!}}\, Y_{\ell m}(\cos\beta)e^{im\phi} \end{aligned}\right\} \qquad (B.5)$$

where

$$P_{\ell m}(\mu) = (1-\mu^2)^{m/2}\frac{d^m}{d\mu^m}P_\ell(\mu) \qquad (B.6)$$

and

$$P_\ell(\mu) = \frac{1}{2^\ell \ell!}\frac{d^\ell}{d\mu^\ell}(\mu^2-1)^\ell \qquad (B.7)$$

$P_{\ell m}(\mu)$ are the associated Legendre Functions

$$\begin{aligned} P_{11}(\mu) &= (1-\mu^2)^{1/2} & P_{31}(\mu) &= \tfrac{3}{2}(5\mu^2-1)(1-\mu^2)^{1/2} \\ P_{21}(\mu) &= 3\mu(1-\mu^2)^{1/2} & P_{32}(\mu) &= 15\mu\,(1-\mu^2) \\ P_{22}(\mu) &= 3(1-\mu^3) & P_{33}(\mu) &= 15(1-\mu^2)^{3/2} \end{aligned} \qquad (B.8)$$

$$Y_{\ell_1 -m}(\theta,\phi) = (-1)^m\, Y^*_{\ell m}(\theta,\phi) \qquad (B.9)$$

Orthogonality Rule for $Y_{\ell m}(\theta,\phi)$:

$$\int_0^{2\pi} d\phi \int_0^{\pi} Y^*_{\ell' m'}\, Y_{\ell m}\sin\theta d\theta = \delta_{\ell\ell'}\delta_{mm'} \qquad (B.10)$$

$$\begin{aligned} Y_{00} &= 1/\sqrt{4\pi} \\ Y_{10} &= \sqrt{\frac{3}{4\pi}}\cos\theta \\ Y_{11} &= \sqrt{\frac{3}{8\pi}}\, e^{i\phi}\sin\theta \end{aligned} \qquad (B.11)$$

$$\left.\begin{aligned} Y_{20} &= \frac{1}{2}\sqrt{\frac{5}{4\pi}}\,(3\cos^2\theta-1) \\ Y_{21} &= \sqrt{\frac{15}{8\pi}}\,e^{i\phi}\,\sin\theta\cos\theta \\ Y_{22} &= \frac{1}{4}\sqrt{\frac{15}{2\pi}}\,e^{2i\phi}\sin^2\theta \end{aligned}\right\} \tag{B.12}$$

Normalized form $\underset{\sim}{\chi}_{\ell m}(\theta,\phi)$ of $\underset{\sim}{L}\, Y_{\ell m}(\theta,\phi)$

$$\underset{\sim}{\chi}_{\ell m}(\theta,\phi) = \frac{1}{\sqrt{\ell(\ell+1)}}\,\underset{\sim}{L}\, Y_{\ell m}(\theta,\phi) \tag{B.13}$$

where

$$\underset{\sim}{\chi}_{o,m} \equiv 0$$

Orthogonality Properties

$$\left.\begin{aligned} \int \underset{\sim}{\chi}^{*}_{\ell' m'} \cdot \underset{\sim}{\chi}_{\ell m}\, d\Omega &= \delta_{\ell'\ell}\delta_{m'm} \\ \int \underset{\sim}{\chi}^{*}_{\ell' m'} \cdot (\underset{\sim}{r} \times \underset{\sim}{\chi}_{\ell m})\, d\Omega &= 0 \end{aligned}\right\} \tag{B.14}$$

$$\int [f_1(Kr)\underset{\sim}{\chi}_{\ell' m'}]^{*} \cdot [g_\ell(Kr)\underset{\sim}{\chi}_{\ell m}]\, d\Omega = f^{*}_{\ell} g_\ell \delta_{\ell'\ell}\delta_{m'm} \tag{B.15}$$

$$\int [f_1(Kr)\underset{\sim}{\chi}_{\ell' m'}]^{*} \cdot [\underset{\sim}{\nabla} \times g_\ell(Kr)\underset{\sim}{\chi}_{\ell m}]\, d\Omega = 0 \tag{B.16}$$

$$\frac{1}{K^2}\int[\underset{\sim}{\nabla} \times f_\ell(Kr)\underset{\sim}{\chi}_{\ell'm'}]^* \cdot [\underset{\sim}{\nabla} \times g_\ell(Kr)\underset{\sim}{\chi}_{\ell m}]d\Omega$$

$$= \delta_{\ell'\ell}\delta_{m'm}\{f_\ell(Kr)^* g_\ell(Kr) + \frac{1}{K^2r^2}\frac{\partial}{\partial r}[rf_\ell^* \frac{\partial}{\partial r}(rg_\ell(Kr)]\} \tag{B.17}$$

APPENDIX C

SPHERICAL WAVE EXPANSION OF A VECTOR PLANE WAVE

It helps to have an expansion of a plane electromagnetic wave in spherical waves when discussing the scattering or absorption of electromagnetic radiation by spherical objects.

For a scalar field $\psi(x)$ satisfying the wave equation the necessary expansion can be obtained by using the orthogonality properties of the spherical solution $j_\ell(Kr)Y_{\ell m}(\theta,\phi)$. One can also use the spherical wave expansion of the Green function $\frac{e^{iKR}}{4\pi R}$. Let $|\underset{\sim}{x}| \to \infty$ on both sides. We can then place $|\underset{\sim}{x}-\underset{\sim}{x}'| = \underset{\sim}{r}'-\underset{\sim}{n}\,\underset{\sim}{x}$ on the left-hand side, where $\vec{n}$ is the unit vector in the $\vec{x}$ direction. On the right side we put $r_2 = r'$ and $r_2 = r$. We can also use the asymptotic form (A.11) for $h^{(1)}(Kr)$. We now have

$$\frac{e^{iKr'}}{4\pi r'} e^{-iK\underset{\sim}{n}\cdot\underset{\sim}{x}} = iK \frac{e^{iKr'}}{Kr} \sum_{m=-\ell}^{\ell} (-i)^{\ell+1} j_\ell(Kr) Y^*_{\ell m}(\theta',\phi') Y_{\ell m}(\theta,\phi) \tag{C.1}$$

By simplification and taking the complex conjugate we have the expansion of a plane wave,

$$e^{i\underset{\sim}{K}\cdot\underset{\sim}{x}} = 4\pi \sum_{\ell=0}^{\infty} i^\ell j_\ell(Kr) \sum_{m=-\ell}^{\ell} Y^*_{\ell m}(\theta,\phi) Y_{\ell m}(\theta',\phi') \tag{C.2}$$

where $\underset{\sim}{K}$ is the wave vector with spherical coordinates. By using the addition theorem

$$P_\ell(\cos\gamma) = \frac{4\pi}{2\ell+1} \sum_{m=-\ell}^{\ell} Y^*_{\ell m}(\theta',\phi') Y_{\ell m}(\theta,\phi) \tag{C.3}$$

Equation (C.2) becomes

$$e^{i\underset{\sim}{K}\cdot\underset{\sim}{x}} = \sum_{\ell=0}^{\infty} i^\ell (2\pi+1) j_\ell(Kr) P_\ell(\cos\gamma) \tag{C.4}$$

where γ is the angle between $\underset{\sim}{K}$ and $\underset{\sim}{x}$. By knowing that

$$Y_{\ell 0}(\theta,\phi) = \sqrt{\frac{2\ell+1}{4\pi}}\, P_\ell(\cos\theta) \tag{C.5}$$

Equation (C.4) is

$$e^{i\underset{\sim}{K}\cdot\underset{\sim}{x}} = \sum_{\ell=0}^{\infty} i^\ell \sqrt{4\pi(2\ell+1)}\, j_\ell(Kr) Y_{\ell 0}(\gamma) \tag{C.6}$$

Now we will make an equivalent expansion for a circularly polarized plane wave with helicity ± incident along the z-axis.

$$\underset{\sim}{E}(\underset{\sim}{x}) = (\underset{\sim}{\varepsilon}_1 \pm i\underset{\sim}{\varepsilon}_2) e^{iKz} \tag{C.7}$$

$$\underset{\sim}{B}(\underset{\sim}{x}) = \underset{\sim}{\varepsilon}_3 \times \underset{\sim}{E} = \pm i\underset{\sim}{E} \tag{C.8}$$

Jackson then finds that the multipole expansion of the plane wave equation is

$$\underset{\sim}{E}(\underset{\sim}{x}) = \sum_{\ell=1}^{\infty} i^{\ell} \sqrt{4\pi(2\ell+1)} \left[j_{\ell}(Kr) \underset{\sim}{\chi}_{\ell,\pm 1} \pm \frac{1}{K} \underset{\sim}{\nabla} \times j_{\ell}(Kr) \underset{\sim}{\chi}_{\ell,\pm 1} \right]$$

$$\underset{\sim}{B}(\underset{\sim}{x}) = \sum_{\ell=1}^{\infty} i^{\ell} \sqrt{4\pi(2\ell+1)} \frac{-i}{K} \underset{\sim}{\nabla} \times j_{\ell}(Kr) \underset{\sim}{\chi}_{\ell,\pm 1} \mp i j_{\ell}(Kr) \underset{\sim}{\chi}_{\ell,\pm 1} \right] \qquad (C.9)$$

So for this circularly polarized wave the m values have obvious interpretation of ± 1 unit of angular momentum per photon parallel to the propagation direction.

VITA

Brenna Kay Russell was born in Murray, Kentucky, on April 17, 1962. She graduated from Oak Ridge High School in 1980. Her Bachelor of Science degree in Engineering Physics was received from The University of Tennessee, Knoxville, in 1984. She received her Master of Science degree with a major in Physics from The University of Tennessee, Knoxville, in December 1986. She is a member of Sigma Pi Sigma.